Chemical Engineering Science 162 (2017) 284–299

Contents lists available at ScienceDirect

Chemical Engineering Science

journal homepage: www.elsevier.com/locate/ces

Agglomeration during spray drying: Airborne clusters or breakage at the walls?

Víctor Francia [a,b,*], Luis Martín [b], Andrew E. Bayly [b,1], Mark J.H. Simmons [a]

[a] School of Chemical Engineering, University of Birmingham, Birmingham B15 2TT, United Kingdom
[b] Procter & Gamble R&D, Newcastle Innovation Centre, Newcastle upon Tyne, United Kingdom

ARTICLE INFO

Article history:
Received 2 August 2016
Received in revised form 1 December 2016
Accepted 15 December 2016
Available online 20 December 2016

Keywords:
Spray dryer
Fouling
Agglomeration
Deposition
Resuspension
Removal

ABSTRACT

Particle agglomeration, wall deposition and resuspension are inherent to many industries and natural processes, and often inter-connected. This work looks into their relation in a confined particle laden swirling flow. It investigates how the size of detergent powder spray dried in a swirl counter-current tower responds to changes in the air flow. Four sets of sprays are investigated under varying combinations of air temperature and velocity that cause the same evaporation. The use of high air velocities accumulates more of the droplets and dry powder in the chamber swirling faster, but it leads to creation of a finer product. Particle-particle and particle-wall contacts are made more frequent and energetic but in turn the swirl troughs the solids to the wall where deposits constantly form and break. Past *PIV* and tracer studies revealed that the rates of deposition and resuspension are balanced; the data discussed here indicate that the dynamic nature of the deposits is a major contributor to particle formation. In contrast with the usual assumption, the product size seems driven not by inter-particle contacts in airborne state but the ability of the solids to gain kinetic energy and break up a collection of clusters layering on the wall. As a result, the dryer performance becomes driven by the dynamic of deposition and resuspension. This paper studies the efficiency of limiting operation strategies and shows that a low temperature design concept is better suited to control fouling phenomena and improve capacity and energy consumption.

1. Introduction

Particle agglomeration is at the core of powder manufacturing. Fluidised beds or granulators (Tan et al., 2006; Fries et al., 2013) are examples of well controlled processes, but particles grow in a more uncontrolled fashion in dryers (Verdurmen et al., 2004) or cyclones (Alves et al., 2015). Agglomeration is regarded as the result of a collision between two flowing particles or droplets (Sommerfeld, 2001). Impacts to the wall of process units or the material layering there receive less attention (Jin and Chen, 2010; Song et al., 2016). Similarly to the treatment of particle-particle contacts (Sutkar et al., 2015) the collisions of dry or wet particles to the walls are simplified by restitution coefficients (Hastie, 2013; Crüger et al., 2016). In most cases, numerical models of particulate processes neglect deposition or assume that it leads to a static layer of material that plays no role in the overall process. In a sense, the lack of an advanced description of fouling is a handicap of the powder industry. Deposition, consolidation, suppression and resuspension are widely studied in other fields such as sediment and soil dynamics (Harris and Davidson, 2009), nuclear (Lustfeld et al., 2014) and heat transfer engineering (Yeap et al., 2004; Bansal and Chen, 2006), microfluidics (Marshall and Renjitham, 2014), membrane technology (Melián-Martel et al., 2012), combustion and ash deposits (Zbogar et al., 2009) or biotechnology (Chu and Li, 2005).

Ziskind (2006), Li et al. (2011) and the work of Henry et al. (2012), and Henry and Minier (2014) set a clear picture of the state-of-the-art in colloidal and particulate fouling research. Many technologies refer to deal with colloids and/or inertia-less systems that form mono-layered deposits (Soldati and Marchioli, 2009) where fouling is treated essentially as a fluid dynamics problem. Many industries however handle cohesive materials and deal with complex multi-layered deposits. Depending on the case, deposits evolve in time due to the transfer of momentum e.g. deposition and removal processes, heat and mass e.g. drying, sintering, or undergoing chemical reactions e.g. ageing. Such a complex behaviour is not exceptional but the rule in energy and environmental engineering (Abd-Elhady et al., 2007; Lecrivain

* Corresponding author at: School of Chemical Engineering, University of Birmingham, Birmingham B15 2TT, United Kingdom.
E-mail address: v.francia.chemeng@gmail.com (V. Francia).
[1] Present address: School Chemical and Process Engineering, University of Leeds, Leeds, United Kingdom.

http://dx.doi.org/10.1016/j.ces.2016.12.033
0009-2509/

Nomenclature

A	cross-sectional area of the cylindrical chamber, m^2
C	capacity ratio $C = 1 - ((M_E + M_R)/M_{EP})$, –
D	diameter of the cylindrical chamber, m
d	diameter of the top exit in the dryer, tubular guard, m
f	normalised size frequency in a probability density function, log (μm)$^{-1}$
H_A	enthalpy rate for the air taking ambient temperature as reference $H_A = \int_{T_{Amb}}^{T_{A,av}} M_A\, c_{p,A}.dT$, J s^{-1}
$\Delta H_{DA,Sn}$	enthalpy variation between outlet and inlet air in a dry basis, J s^{-1}
$\Delta H_{p,Sn}$	enthalpy variation between the outlet product, elutriates and water vapour and the inlet slurry, J s^{-1}
M	mass rate, kg s^{-1}
M_S	mass rate of slurry sprayed at the nozzle, kg s^{-1}
M_E	mass rate of powder elutriated and collected at the cyclones, kg s^{-1}
M_R	mass rate of oversized product exiting the tower belt, kg s^{-1}
M_P	mass rate of the product exiting the tower belt, kg s^{-1}
M_{EP}	overall rate of powder exiting the spray drying chamber, kg s^{-1}
Oh^2	Ohnesorge number, $Oh^2 = 2\mu_p{}^2/x_p\, \rho_p\, \sigma_p$
Q_{Lat}	latent enthalpy rate of the water vapour generated in the chamber, J s^{-1}
Q_{Loss}	rate of heat lost to the environment, J s^{-1}
Q_{Ex}	rate of heat exchanged in the dryer, J s^{-1}
Q_S	rate of heat transferred to the solid phase, J s^{-1}
q	specific heat transfer rate per m and kg of dry slurry, kJ m^{-1} kg$_{DS}^{-1}$
$r_{d,o}$	initial net wall deposition rate, g m^{-2} s^{-1}
rH_A	relative humidity of the air, %
T	time averaged temperature, °C
$T_{A,av}$	cross-sectional average air temperature, $T_{A,av} = \int \rho_A U_{A,z} T_A\, dA \,/\, \int \rho_A U_{A,z} dA$ where normalised radial profiles for $U_{A,z}$ are taken from isothermal cases (Francia et al., 2015c)
U	time averaged velocity, m s^{-1}
U_{av}	bulk or superficial air velocity, m s^{-1}
$U_{p,Sd}$	particle sedimentation or free falling velocity, m s^{-1}
$U_{p,t}$	particle terminal velocity, m s^{-1}
$U_{p,w}$	particle velocity for the first wall impact, m s^{-1}
X_w	product water mass fraction
z	axial position in the cylindrical chamber measured from the level of the air inlets, m

Greek letters and symbols

η_t	thermal efficiency in the dryer, $\eta_t = (T_{A,IN} - T_{A,EX})/(T_{A,IN} - T_{amb})$
η_h	heat transfer efficiency in the dryer, $\eta_h = Q_S/H_{A,IN}$
Ω_i	design swirl intensity, non-dimensional flux of angular momentum (Francia et al., 2015c)

Subscripts, superscripts and caps

A	for the air phase
DA	for dry air
DS	for dry slurry
E	for the elutriated fraction of powder
EP	for the full powder exiting the tower (elutriated fraction + product from the bottom)
EX	exhaust conditions
IN	inlet conditions
P	for the particle/product exiting the tower from the bottom end
R	for the fraction of oversized powder removed from that exiting from the tower belt

et al., 2014; Diaz-Bejarano et al., 2016; Alipour et al., 2016), or in materials and powder industries (Adamczyk et al., 2008; Batys et al., 2015; Nakazato, 2015). Studies of multilayered deposits include analysis of stress propagation (Bourrier et al., 2010), clustering (Tanaka et al., 2002; Iimura et al., 2009), kinetic frames (Zhang et al., 2013) and advance experimental set ups (Barth et al., 2013), but in many practical cases, data are scare and engineers cannot predict how fouling responds to operation conditions. This limitation compromises the efficiency in handling powders (e.g. detergents, ceramics, biomass, foods, pharmaceutics) and intensifying their production (e.g. dryers, granulators, mixers, burners, fluidized beds, conveyors).

Spray dryers are particularly challenging because they bring together dry particles with semidried and wet droplets. Our past work studied the origin of agglomeration in swirl countercurrent towers and described how the placement of nozzles (Francia et al., 2016a, 2016b) affects the process. *PIV* studies (Hassall, 2011) and a set of tracer experiments (Francia et al., 2015a) also demonstrated that in drying detergent formulas the deposits generated are dynamic structures constantly forming and breaking. One in five particles were found to be the direct result of deposit resuspension but the data suggested many more interact at the wall without becoming permanently fixed. This opens an interesting debate on whether the contacts leading to agglomeration take place in airborne state or at the walls and in how the drying conditions can be used to control them. To answer some of these questions, this paper studies the effect of changing the air properties on the agglomeration in swirl drying towers. It investigates the response of four nozzle configurations previously reported in a reference case (Francia et al., 2016a, 2016b) to varying air flow conditions. The focus is placed in establishing the combined effect of changing the temperature and momentum of the air flow. Two limiting strategies are compared: (a) high temperature (e.g. weak but hot air vortex), or (b) high velocity (e.g. strong but cold air vortex). The trends observed along the support of visualization and tracer studies suggest that agglomerates form by breakage of wallborne clusters rather than by airborne contacts. Accordingly, design concepts based in a high air velocity at low temperature seem better suited to use the kinetic energy of the solids to control the final particle size and the energy efficiency.

2. Agglomeration during spray drying

2.1. Traditional description: airborne phenomena

Agglomerates are regarded as the result of two flowing particles or droplets coming together. Most research in spray drying focuses in finding when and where in a dryer e.g. distance from the nozzle, the surface of a droplet dries sufficiently to prevent growth. Two particles/droplets are said to adhere if they come in contact for long enough to form a viscous bridge and/or let amorphous substances sinter (Palzer, 2011). Thus major efforts are made to quantify the ability of a drying droplet to stick (Adhikari et al., 2003, 2005) and link it to surface properties e.g. viscosity <10^8 Pa s, surface tension or liquid-solid contact angle. Properties

of the amorphous substances e.g. shear viscosity, viscoelasticity, glass transition temperature, are used as a guide to study the tendency for agglomeration (Palzer, 2009) and the generation of structure (Palzer et al., 2012). Transition through a glass state also serves to characterise additives (Wang and Langrish, 2009) and delimit the regions of a dryer where solids are prone to agglomerate (Gianfrancesco et al., 2009; Malafronte et al., 2015) or deposit (Woo et al., 2010). Most available work deals with food and co-current dryers. In this field, computational fluid dynamic frames are common (Kuriakose and Anandharamakrishnan, 2010); they make use of single droplet drying models (Mezhericher et al., 2008; Handscomb and Kraft, 2010) to predict heat and mass transfer rates and relate the particle flux to the wall to deposition assuming a fraction of it forms static layers of material (Kota and Langrish, 2007; Jin and Chen, 2010; Sadripour et al., 2012; Keshani et al., 2015). In a dryer, rates of mass, heat and momentum transfer are strong functions of particle size, which in addition to the issue of scale make the description of particle interactions a substantial challenge. It is tackled by the application of stochastic collision models that estimate the rate of inter-particle contacts in the air flow (Nijdam et al., 2006; Mezhericher et al., 2012). Yet, models often struggle to be validated when growth is significant (Langrish, 2009; Palzer, 2011). The account of the contact mechanics between viscous droplets has improved drastically over the last decade in experimental (Kuschel and Sommerfeld, 2013; Pawar et al., 2016) and numerical aspects (Focke et al., 2013), but some practical difficulties remain in using material properties easy to measure in slurries or powders but hard in semi-dried matter (Boonyai et al., 2004; Werner et al., 2007).

Counter-current dryers are used to produce thermally stable powders e.g. detergents, ceramics, and often incorporate the use of swirl. Detergents are particularly complex cases due to their formulation including surfactant(s), polymer(s), inorganic salt(s) and others. Since only some components undergo a glass transition the usual approach in foods not applicable. The counter air flow and the swirl also complicate the system by increasing the concentration of solids and multiplying particle interactions. Given this complexity, the large scale and a difficult access, swirl towers are less well known than co-current chambers. Only few authors have studied them experimentally in pilot scale and reported temperature fields and product properties (Fieg et al., 1994; Zbicinski et al., 2002; Zbicinski and Piatkowski, 2009). Despite the complex swirling flow, stochastic agglomeration models have also been implemented in CFD models of swirl towers or cyclones (Paiva et al., 2010; Jaskulski et al., 2015). More often, numerical works study the flow patterns (Harvie et al., 2001; Wawrzyniak et al., 2012) and drying rates (Harvie et al., 2002; Ali et al., in press) but struggle to predict the performance without describing agglomeration accurately. In manufacturing dryers and beyond the issue of scale, models face two major challenges: describing the effect of fouling and wall roughness in increasing the particle residence time (Francia et al., 2015a) and a complex flow structure largely determined by the effects of friction in swirl stability (Francia et al., 2015c, 2015d), both phenomena yet to be reproduced numerically. Subsequently and before going into a realistic representation of this process, recent works turn back to a more rigours study of how multi-phase flow models actually perform in large confined vortex flows looking at the dispersion of glass beads in isothermal cases at low level of friction (Ali et al., 2017). In summary, the control of product size and its effects on design/operation rules in counter-current drying towers remains largely unexplored. When one increases production rate, particle growth comes to limit capacity and efficiency (Huntington, 2004). Typical dryer designs minimise the number of contacts with the placement of sprays (Davis et al., 1971) but growth must be optimised rather than avoided.

2.2. Study of wallborne phenomena

Wall deposition has been thoroughly studied in co-current dryers, particularly foods. It is associated to a loss in yield and safety and quality issues (Kota and Langrish, 2006; Keshani et al., 2015). The resuspension of deposits has been pointed at (Hanus and Langrish, 2007a, 2007b) but not yet quantified or related to an effect in the process. It remains unclear whether the deposits in co-current and nil-swirl dryers are in truth static, or to which extent they affect particle formation or residence time. In a swirl tower little attention has been paid to fouling. The work of Hassall (2011) was the first in showing that most of the powder concentrates in an annular region near the wall, Fig. 1a (Hassall, 2011). Here, air-borne particles interact with those fix at the deposits, Fig. 1b (Hassall, 2011), forming and breaking clusters of different size and shape, which then roll, deposit, pick up material, break or detach. For decades the phenomenon was known but it

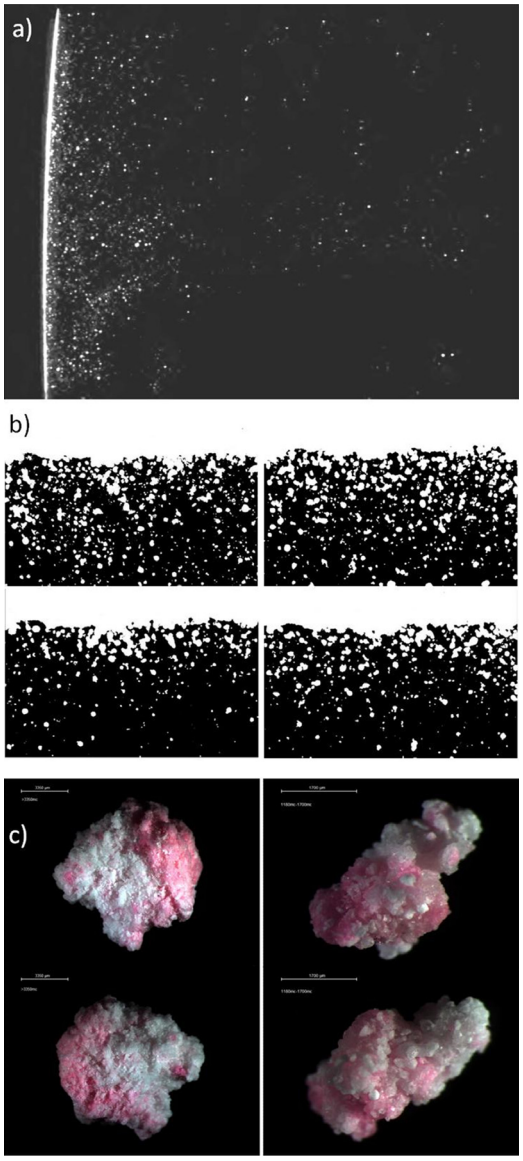

Fig. 1. Visualization of the wall dynamics: (a) and (b) show the near wall region and multi-layered deposits observed under Particle Image Velocimetry, *PIV*, reproduced from Hassall (2011). (c) Granules >850 during S_2 whereby the colour tracer tracks material resuspended from the deposits (Francia et al., 2015a). (For interpretation of the references to colour in this figure legend, the reader is referred to the web version of this article.)

was belief that only large pieces could detach (Huntington, 2004). Recent tracer experiments (Francia et al., 2015a) urge to reconsider this view providing evidence that deposits are in fact dynamic structures. The layers of clusters shown in Fig. 1b renew continuously releasing clusters varying from tens of micrometers to millimetres. The coarsest granules in the product are shown to form at the wall structure by agglomeration of deposits with wet droplets (e.g. Fig. 1c shows granules examples where a dye tracks the resuspended material, Francia et al., 2015a). The exchange of material at the wall has a remarkable impact in the process since >20% of the product comprises of resuspended material that dries at the wall for 10–100 times longer than flowing in the air (Francia et al., 2015a). Not considering the time that the product remains at the wall and the processes undergone there explains the difficulties of past approaches to predict drying rate or particle size. In summary, the walls have revealed as a much more relevant actor than anticipated at least in counter-current swirl dryers and it is now important to find ways to account for them at a design stage. It is needed to understand deposition and removal processes and ideally, predict the time the solids remain in wall structures (Fig. 1b) and any growth rate resulting from the different sizes of the droplet/particles coming in and out.

3. Experimental methodology

This paper examines the effect of the air flow conditions in the agglomeration observed in a full scale swirl spray drying tower of detergent property of Procter & Gamble. It compares the operation of four spray arrangements described in the past under a reference air flow ~ (Francia et al., 2016a, 2016b), with the operation under the same inlet properties for the solids but drastic changes in the air conditions, + and −. It expands the initial data reported at international conferences (Francia et al., 2015b) with a full account of operation, deposition, temperature fields, energy efficiency and multi-nozzle operation.

3.1. Unit design

Fig. 2 depicts the dryer and the location of sprays. Hot air is injected with angular momentum into the bottom, moves upwards in swirling motion and exits from the top. The slurry is atomized in one or two swirl pressure nozzles that form a hollow cone spray. The finest powder is elutriated with the air and collected in cyclones. A fraction of the spray is initially elutriated up but then migrates to the wall due to the swirl. Most of the solids however are sufficiently coarse to reach the wall below the nozzle level, where they concentrate and start settling in swirling motion. When using two spays the material flowing up from the bottom is captured by the top spray; it grows and starts flowing down (Francia et al., 2016b). Deposits form near the projection of the spray(s), see Fig. 2. Here, the wall receives the impact of (a) powder that falls swirling at terminal velocity and saltating at the wall and (b) wet droplets coming from the nozzle at high velocity. Interaction with the outer layers (Fig. 1b) makes some of these solids to deposit, others to rebound and others to pick up material, roll and grow as they settle (Hassall, 2011; Francia et al., 2015a). For a detailed description of dispersion and the unit compartmentalization in modelling frameworks, interested readers are referred to Francia et al. (2016a, 2016b).

3.2. Measurements and monitoring the drying chamber

Droplet size was measured with laser diffraction in an external rig (Sympatec GmbH HELOS/BR - Rodox, Lenses R2, R4 R7, details in Francia et al. (2016a)). The elutriation rate was monitored at

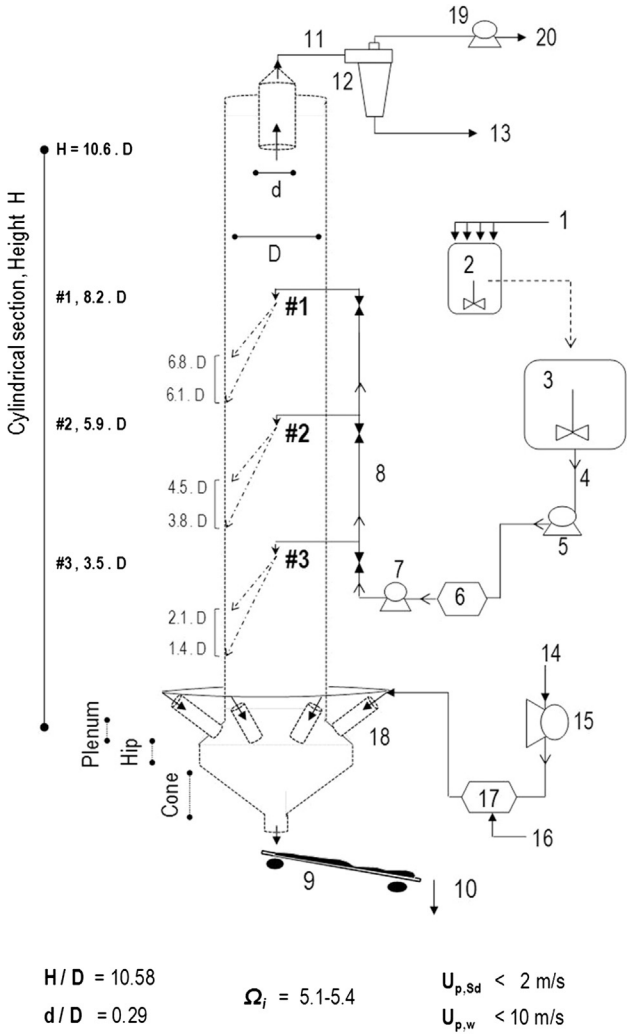

Fig. 2. Outline of a counter-current spray drying tower. Nomenclature, hot air injection, slurry preparation, location of nozzles and projection of the sprays at the walls.

the exit of the cyclones. Product samples were taken at the tower belt, '9' in Fig. 2, where an infrared probe (OMEGA OS551) measures the powder temperature, T_P. Ten samples were used for analysis of size under sieving. A larger bulk sample was taken and sieved into eleven classes (Russell Finex Model 17240) used for analysis of water content (Toledo Mettler Moisture Balance). Sampling or humidity measurements inside the dryer are extremely

hard due to the deposition of solids on any large probe. Zbicinski et al. (2002) propose a device to extract air and measure temperature T_A and humidity, rH_A after filtering the solids. A similar design was successfully tested here but data collection was perhaps too time-consuming for a wide study. Experiments in large scales are expensive and production needs to be minimised. With this in mind, in situ measurements were limited to air temperature and deposition rate at the locations shown in Fig. 3a. The initial net deposition rate $r_{d,o}$ is computed weighting the deposits formed over a clean inspection area in 10–15 min. The air temperature, T_A, was monitored at the inlet, tt-0, and exhaust lines, tt-5. Inside the cylinder, T_A, was tracked automatically by K-type thermocouples placed inside four hollow metallic bars aligned with the radius of the chamber. Each bar exposed sensors to the flow at seven small rectangular openings, Fig. 3d. As suggested by Huntington (2004), deposition and condensation were avoided aligning these openings in the shadow of the swirl and placing the bars sufficiently far from the spray(s). Data obtained in this way were in agreement with the exhaust probe (tt-5) in the absence of solids and similar T_A and rH_A. At the cone T_A was measured manually with a single thermocouple (t-c).

In order to heat up the metal structure, the unit starts up by initiating the burner and the inlet fans blowing hot air into the dryer; when atomization starts, the inlet air rate and temperature, M_A and $T_{A,IN}$, are stepwise increased to target values. In full scale, it takes a long time to heat up the chamber but it is crucial to ensure that steady heat losses are reached before sampling. One cannot afford to operate for many hours to inspect multiple measurements of product water content X_w; instead one may use the temperature of the dryer wall to monitor the evolution of the heat losses i.e. constant heat losses imply a constant wall temperature. The end of start-up period was set according to the stabilization of the wall temperature T_{wall} at the tower bottom (Fig. 3c). Sampling and measurements were taken after T_{wall} remained constant (<0.5 °C/min), which ultimately resulted in constant values for X_w.

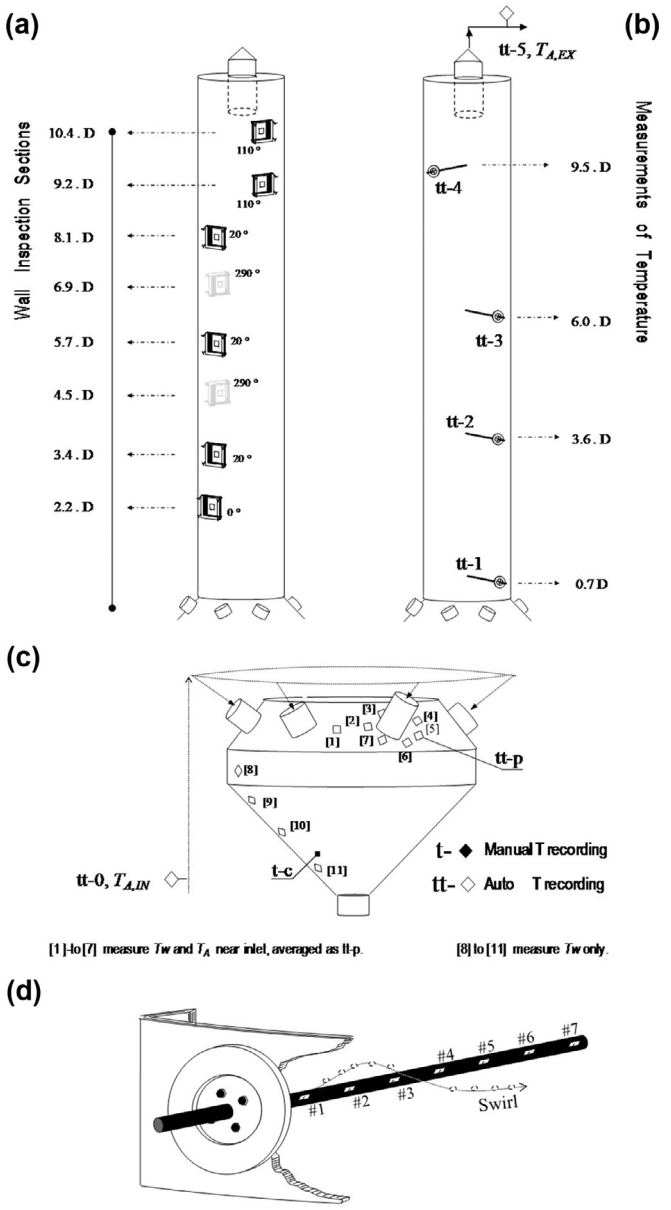

Fig. 3. Measurements: (a) wall inspection areas, (b) air temperature, T_A sensors in the cylinder and exhaust line, (c) T_A sensors at inlet, bottom sections and at the walls, T_W, and (d) arrangement of thermocouples inside hollow bars.

3.3. Two limiting operation strategies

For a given formulation, a swirl tower can be controlled by modifying either the injection of the slurry:

- Changing the slurry rate, M_S (i.e. atomization temperature, pressure or nozzle type and number).
- Using a different injection configuration (i.e. number and location of nozzles).
- Modifying the droplet size (i.e. atomization temperature, pressure or nozzle type).

Or the properties of the inlet air flow:

- Modifying the inlet air rate, M_A.
- Modifying the inlet air temperature, $T_{A,IN}$.

Manufacturers usually try to maximise the rate of slurry M_S that may be dried under a fix set of nozzles. The effect of modifying the location and number of nozzles has been described elsewhere (Francia et al., 2016a, 2016b). In practise, once atomization conditions are fixed, the only way to manipulate the process is finding an optimum balance in the air conditions: mass rate M_A and temperature, $T_{A,IN}$. Put simply, one can modify temperature and adjust the rate to cause the same heat and mass transfer e.g. if one reduces $T_{A,IN}$ it is necessary to increase the rate M_A to dry the product, and vice versa. Two limiting strategies arise: high air temperatures at a low rate (e.g. hot weak vortex) or high rate at low temperatures (e.g. cold strong vortex) leading to:

- *Different flow patterns*: An increase in the rate M_A originates higher air velocities U_A in the dryer and as a result the powder concentrates and experiences a longer residence time.
- *Different heat and mass transfer kinetics*: An increase in the rate M_A must be accompanied by a drop in the air temperature to keep a constant evaporation rate. As a result, higher velocities and lower temperatures have competing effects in the local heat transfer rate since they reduce the ΔT between the phases (particularly at the bottom, Section 4.3) and better convection in areas of high air velocity.

This work compares both strategies studying the same nozzle configuration, rate and atomization conditions reported in Francia et al. (2016a, 2016b) but increasing and decreasing $T_{A,IN}$ by 40 °C while M_A is adjusted to cause the same evaporation. Operation conditions are summarized in Table 1 where ~ denotes the reference operation taken from Francia et al. (2016a, 2016b) and

Table 1
Process conditions for the air and slurry/particulate phase. Comparison of the reference case ~ taken from Francia et al. (2016a, 2016b) with a cold strong vortex − ($\downarrow T_A \uparrow U_A^2$) and a hot weak vortex + ($\uparrow T_A \downarrow U_A^2$). Intervals denote ± 2$\sigma$.

Case		S_{-1}	$S_{\sim 1}$	S_{+1}	S_{-2}	$S_{\sim 2}$	S_{+2}
Air phase							
Nozzle/s		#1	#1	#1	#2	#2	#2
$M_S/M_{S,S\sim 1}$		1.04 ± 0.02	1.00 ± 0.04	1.0 ± 0.04	0.93 ± 0.04	1.00 ± 0.06	0.93 ± 0.02
$T_P - T_S$	(°C)	15.0 ± 7.0	−4.7 ± 6.8	27.0 ± 8.2	17.3 ± 9.8	−1.4 ± 9.2	21.3 ± 12.8
$X_w - X_{w,S\sim 1}$	(%)	0.7	0.0	1.4	0.6	−0.7	0.6
M_E	(% M_{EP})	5.5	4.0	2.7	3.5	2.7	1.8
M_R	(% M_{EP})	5.6	8.5	18.7	1.6	5.2	7.1
C	(% M_{EP})	88.9	87.5	78.6	94.9	92.0	91.1
Particulate phase							
$M_A/M_{A,S\sim 1}$		1.28 ± 0.04	1.00 ± 0.02	0.86 ± 0.06	1.16 ± 0.08	1.00 ± 0.02	0.84 ± 0.10
tt-0, $T_{A,IN}$	(°C)	229.5 ± 2.4	272.2 ± 4.2	311.4 ± 3.2	230.1 ± 6.2	273.0 ± 3.4	310.7 ± 11.2
tt-5, $T_{A,EX}$	(°C)	79.0 ± 1.6	81.7 ± 1.0	85.0 ± 1.2	78.6 ± 2.0	86.8 ± 1.0	85.7 ± 1.6
$rH_{,EX}$	(%)	19	20	21	19	17	19
Case		S_{-3}	$S_{\sim 3}$	S_{+3}	M_{-13}	$M_{\sim 13}$	M_{+13}
Air phase							
Nozzle/s		#3	#3	#3	#1, #3	#1, #3	#1, #3
$M_{S,\#1}/M_{S,S\sim 1}$		–	–	–	0.99 ± 0.02	0.90 ± 0.02	0.99 ± 0.02
$M_{S,\#3}/M_{S,S\sim 1}$		1.00 ± 0.04	0.99 ± 0.02	0.99 ± 0.02	0.96 ± 0.02	1.01 ± 0.02	0.99 ± 0.02
$T_P - T_S$	(°C)	0.9 ± 9.4	−2.5 ± 8.6	7.5 ± 14.8	34.0 ± 13.6	2.8 ± 3.7	32.7 ± 10.6
$X_w - X_{w,S\sim 1}$	(%)	2.9	4.5	2.9	−0.1	0.7	2.0
M_E	(% M_{EP})	4.1	2.0	2.3	5.1	3.1	1.5
M_R	(% M_{EP})	22.2	27.0	26.1	7.2	11.6	18.2
C	(% M_{EP})	73.7	71.0	71.6	87.7	85.3	80.3
Particulate phase							
$M_A/M_{A,S\sim 1}$		1.28 ± 0.04	0.99 ± 0.02	0.87 ± 0.04	1.94 ± 0.06	1.53 ± 0.06	1.30 ± 0.06
tt-0, $T_{A,IN}$	(°C)	230.3 ± 2.8	269.3 ± 4.6	310.4 ± 5.2	260.0 ± 4.8	300.1 ± 7.0	339.5 ± 6.6
tt-5, $T_{A,EX}$	(°C)	91.2 ± 0.8	89.8 ± 3.4	95.6 ± 1.0	77.0 ± 1.8	78.2 ± 2.2	75.4 ± 1.2
$rH_{,EX}$	(%)	11	14	13	26	29	37

A: air, IN: inlet, EX: exhaust, S: slurry, P: powder at the exit belt, E: powder at the cyclones, R: powder removed as oversized, EP: full rate of spray dried powder.

+ and − denote the operation at higher or lower air inlet temperatures $T_{A,IN}$. The cases denoted S_1, S_2 and S_3 use a single nozzle from positions #1, #2 or #3 in Fig. 2 (Francia et al., 2015b; Francia et al., 2016a); the multi-level production, M_{13}, doubles the slurry rate using simultaneously nozzles #1 and #3 (Francia et al., 2016b).

All cases result in similar exit product water content X_w, Section 4.9. In some instances, Table 1 shows a difference between the product exit temperature T_P in reference and the cases + and −. It responds to a seasonal difference in cooling across the transport belt in Fig. 2. It is a common observation and it has been confirmed by replication of $M_{\sim 13}$ under the same ambient conditions than M_{+13} and M_{-13} leading to the same product properties and T_P. The propagation of this uncertainty along other measurement errors in the mass and energy balances is reflected in the ranges given.

4. Results and discussion

4.1. The decay of the vortex momentum

Each strategy renders a different range of velocities in the chamber. When a single nozzle is used, the lowest inlet temperature − carries associated an increase in inlet air superficial velocity U_{av} of 8–20%, while in a hot vortex + it reduces by 6–9%. The axial momentum flux $\rho_A U_{av}^2$ in turn increases by 26–56% or reduces by 18–23% respectively. When two nozzles are used, M_{13}, the tower operates overall at a higher velocity due to the need of increasing the overall heat transfer rate. From M_{-13} to M_{+13} the velocity and the momentum flux rise by 47–93% and 192–375% respectively. Considering the ratio between the tangential and axial velocity in the outer part of the vortex is in the order of 1–3 (Francia et al., 2015c, 2015d), the energy contained in the tangential motion increases drastically from the hot to the cold cases. Such changes will have significant effects on the ability of the air flow to suspend the powder and bring it to the wall i.e. the powder tends to concentrate further and swirl at higher velocity in the cold scenario.

The air velocity, both in the swirl and axial directions, decays drastically as it rises in the tower due to wall friction, interaction with the solids and the change in density caused by the evaporation. Conversely, the concentration of the powder and its centrifugal inertia increase as the solids move down. To illustrate this effect, Table 2 summarises the differences in superficial air velocity U_{av} and momentum $\rho_A U_{av}^2$ across all cases at different axial locations based on the measured change in air density. Provided that every nozzle injects droplets with the same size, the changes described in Table 2 shall have a major effect in the powder settling velocity i.e. a stronger drag in the axial direction leads to a higher concentration, and in its centrifugal inertia i.e. stronger drag in the tangential direction promotes the migration to the wall.

4.2. Elutriation and capacity

Table 1 includes measurements of the elutriation rate M_E, and the fraction of the product that is too coarse and must be discarded M_R (i.e. computed here as $x_p > 1800$ μm). Both, elutriation of fine particles and production of coarse granules are detrimental to the unit capacity and energy efficiency: in essence, a part of the energy input is used in drying powder that is ultimately discarded. The capacity ratio C computes the fraction of usable product from the overall rate of spray dried powder M_{EP} exiting the chamber. Using a single nozzle, one obtains maximum capacity at an intermediate height, $S_{\sim 2}$ (Francia et al., 2016a), while the transition into two levels in $M_{\sim 13}$ reduces C due to the loss of fine powder (Francia et al., 2016b). The use of different operation strategies has a remarkable effect, Table 1. The axial drag increases substantially from using of a hot weak vortex to a cold strong one i.e. see the rise

Table 2
Axial variation of the air superficial velocity, ($U_{av} = M_A/\rho_A\ \pi R^2$) and axial momentum flux ($\rho_A\ U_{av}^2$) due to the density change. Bold denotes the level taken as reference.

Case		S_{-1}	S_{+1}	S_{-2}	S_{+2}	S_{-3}	$S_{\sim 3}$	S_{+3}	M_{-13}	$M_{\sim 13}$	M_{+13}
Level		Variation in superficial air velocity $U_{av}/U_{av,S3,tt-0}$									
Inlet	tt-0, 0.0 D	1.20	0.94	1.08	0.91	1.20	**1.00**	0.94	1.92	1.62	1.47
N #3 →	tt-1, 0.7 D	1.05	0.75	0.95	0.75	1.02	0.78	0.66	1.58	1.27	1.06
N #2 →	tt-2, 3.6 D	0.96	0.71	0.84	0.61	0.86	0.67	0.59	1.38	1.07	0.91
N #1 →	tt-3, 6.0 D	0.89	0.63	0.75	0.56	0.86	0.67	0.59	1.34	1.05	0.88
	tt-4, 9.5 D	0.83	0.57	0.75	0.56	0.86	0.67	0.59	1.27	0.99	0.84
Level		Variation in axial momentum flux $\rho_A\ U_{av}^2/\rho_A\ U_{av,S3-tt0}^2$									
Inlet	tt-0, 0.0 D	1.54	0.81	1.26	0.77	1.54	**1.00**	0.82	3.75	2.50	1.92
N #3 →	tt-1, 0.7 D	1.35	0.65	1.11	0.63	1.31	0.78	0.58	3.09	1.96	1.38
N #2 →	tt-2, 3.6 D	1.24	0.61	0.98	0.51	1.10	0.67	0.52	2.69	1.65	1.19
N #1 →	tt-3, 6.0 D	1.15	0.55	0.88	0.47	1.10	0.67	0.52	2.61	1.61	1.15
	tt-4, 9.5 D	1.08	0.50	0.88	0.47	1.10	0.67	0.52	2.48	1.52	1.09

of U_{av} from + to ∼ and −, Table 2; as a result more of the powder is elutriated i.e. M_E increases from + to ∼ and −, Table 1. However the capacity C does not decrease as expected but it is maximised thanks to the creation of fewer coarse granules i.e. M_R drops from + to ∼ and −, Table 1. The following sections analyse the heat exchanged in the chamber and the trends in the product size distribution to explain this behaviour and describe the benefits of each strategy.

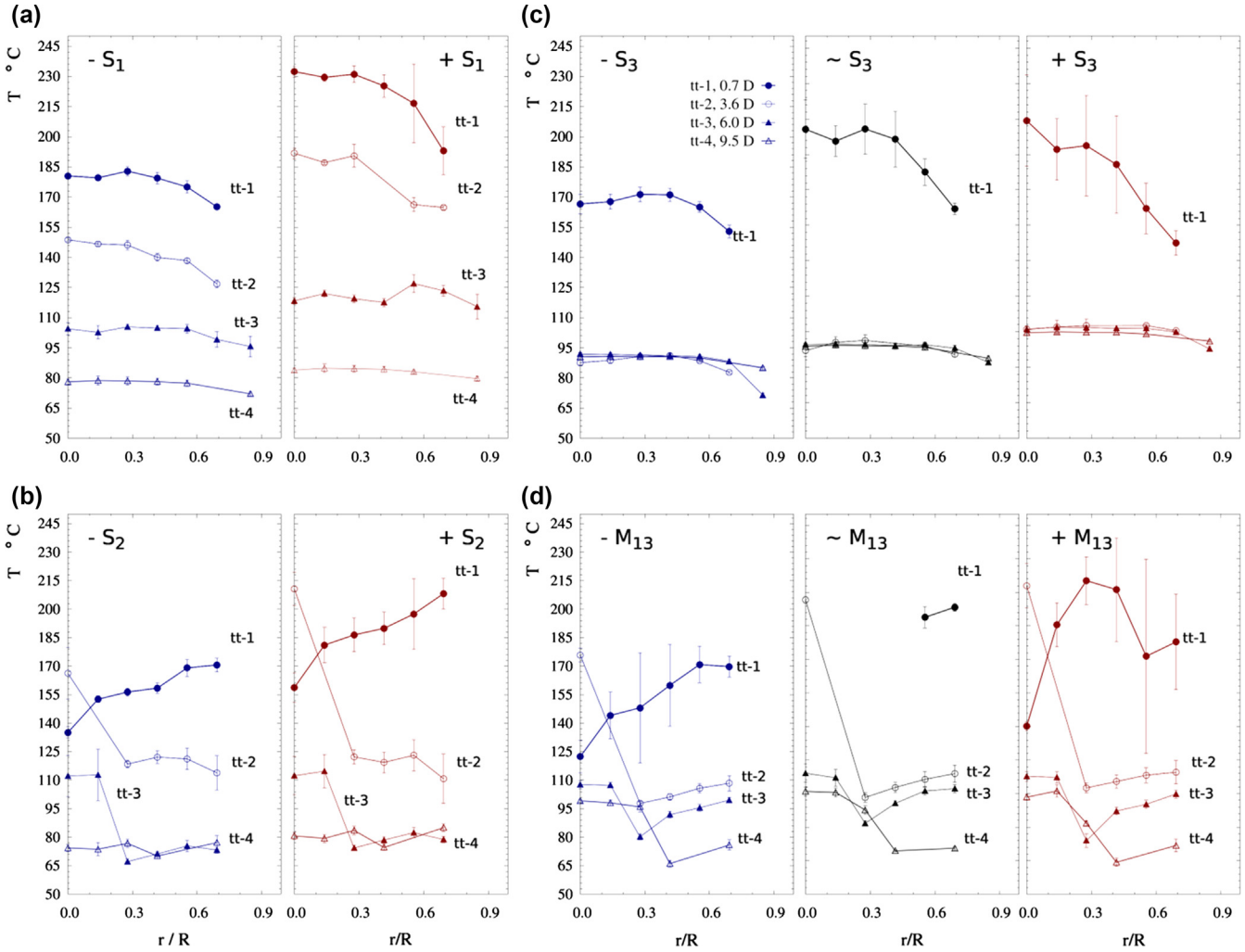

Fig. 4. Time averaged air temperature T_A radial profiles for *tt*-1 at 0.7 D, *tt*-2 at 3.6 D, *tt*-3 at 6.0 D, *tt*-4 at 9.5 D. (a) Operation of nozzle #1 at 8.2 D, (b) operation of nozzle #2 at 5.9 D, (c) operation of nozzle #3 at 3.5 D, and (d) operation from nozzles #1 and #3.

4.3. The drying environment

As a droplet dries and turns solid it becomes less prone to stick; hence its ability to deposit or agglomerate relates to its drying history. Fig. 4 reports the radial temperature profiles in the chamber at different levels and Fig. 5 computes the cross-sectional average $T_{A,av}$ based in normalised velocity profiles. The migration of the solids to the wall originates a radial gradient. When the nozzle is located at a high position (S_1, Fig. 4a) a large span, $\Delta T_A > 30$ °C, appears at the bottom end where T_A decreases close to the wall; instead, the upper section show a flat profile. Moving from a cold to a hot vortex, S_{-1} to S_{+1}, the increase in inlet temperature ($T_{A,IN}$ rises 80 °C) translates in an increment of $\Delta T_A \approx 40$ °C at tt-1, Fig. 4a and $\Delta T_A \approx 20$ °C below the spray level, tt-3 (Fig. 4a). Such a small impact owes to the increase in the heat losses in the distributor when the temperature rises (i.e. drop between $T_{A,IN}$ at tt-0 in Table 1 and tt-p in Fig. 5). From a lower nozzle position (S_2, Fig. 2b) T_A develops a larger span $\Delta T_A > 50$ °C (tt-1, Fig. 4b) and the increase of inlet temperature from S_{-2} to S_{+2} originates only a rise of $\Delta T_A \approx 20$–40 °C at tt-1 and none above. In this case, the air flow field is characterised by a region of high temperature at the centre of the chamber; it appears below the spray projection (tt-2) and survives above (tt-3). When the spray is brought to further down (S_3, Fig. 4c) the entire chamber above the nozzle reaches an homogeneous temperature and the section below the spray projection shows a change in pattern (tt-1, Fig. 4c): T_A reaches a maximum between $0.30 < r < 0.50$ R and decreases at the wall. Interestingly, near the spray T_A rises from S_{-3} to $S_{\sim 3}$ but it does not from $S_{\sim 3}$ to S_{+3} despite the increase in $T_{A,IN}$; only the radial span is affected.

A two-level system M_{13} (Fig. 4d) develops the same hot region observed in S_2. It appears between both nozzles and extends all the way to the top. Features of this type may be linked the destabilization of the vortex under friction observed at isothermal cases with no sprays (Francia et al., 2015c, 2015d). During operation however the vortex stability and thus the location of the recirculation areas will be also affected by the spray momentum, the density gradients and the solid phase. Once *CFD* models are capable to reproduce the swirl decay and the effect of friction for simple cases (Francia et al., 2015c, 2015d) they could be powerful tools to study the origin of this sort of hot spots.

4.4. Distributed energy balance

The evaporation and the heat loss rate are computed from a general mass balance, and the energy balance:

$$Q_{Ex} = Q_{Lat} + Q_{Loss} = -(\Delta H_{DA,sn} + \Delta H_{P,sn}) \quad (1)$$

where Q_{Ex} is defined as the heat rate exchanged between the dry air and the slurry/solids phase. Q_{Ex} represents the variation in sensible enthalpy for a stream of dry air, $\Delta H_{DA,sn}$ (e.g. variation from inlet to exhaust dry air) and the streams containing the injected slurry $\Delta H_{P,sn}$ (i.e. variation from inlet slurry to the combined exit streams of product, elutriated powder and exit water vapour excluding vaporization heat). In this form, the heat exchanged Q_{Ex} is utilised in the latent heat for evaporation, Q_{Lat}, and in the losses through the chamber walls, Q_{Loss}.

All experiments show substantial losses, $Q_{Loss} = 0.29$–0.41 Q_{Ex}; they are negligible above the nozzle and mainly localised in Section I, Fig. 6a (i.e. $Q_{Loss,I} > 0.77$–0.93 Q_{Loss}), particularly within the air distributor (i.e. ΔT_A between tt-0 and tt-p is responsible of 0.63–0.87 Q_{Loss}). To study the drying history of the solids, it is useful to rearrange terms in Eq. (1) and compute the overall enthalpy change of the solid/vapour system, or in other words, the heat transferred into the inlet slurry, Q_S, given below for a section i:

$$Q_{S,i} = -(\Delta H_{DA,sn,i} + Q_{Loss,i}) = Q_{Lat,i} + \Delta H_{P,sn,i} \quad (2)$$

Q_s is utilised in heating and drying the solids. To compute $Q_{s,i}$ across different sections one performs mass and energy balances to each section starting from the injection point. The heat loss rate, which

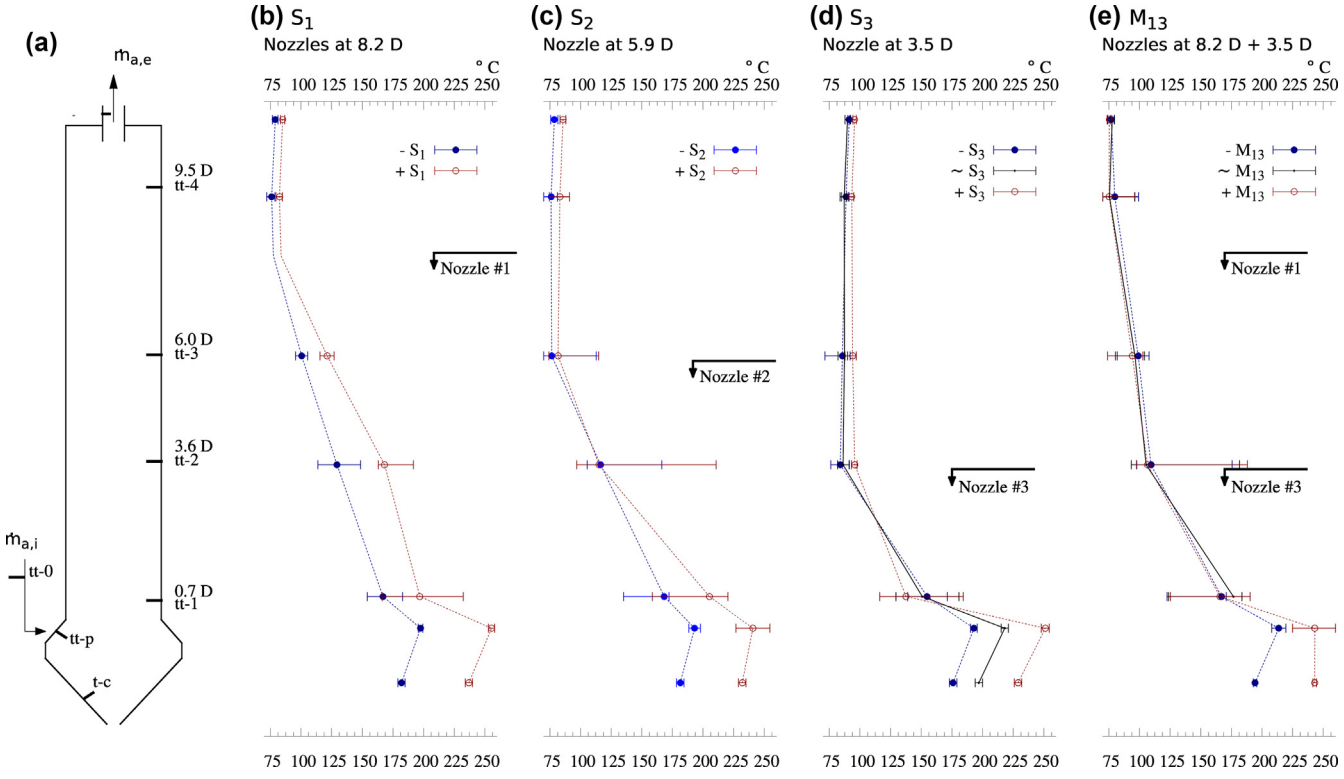

Fig. 5. Cross-sectional average $T_{A,av}$ from *tt*-1 to *tt*-4, time averaged T_A measurements in *tt-p* and single punctual T_A, measurements in *t-c*. (a) Location of sensors, (b) operation of nozzle #1 at 8.2 D, (c) operation of nozzle #2 at 5.9 D, (d) operation of nozzle #3 at 3.5 D, and (e) operation from nozzles #1 and #3.

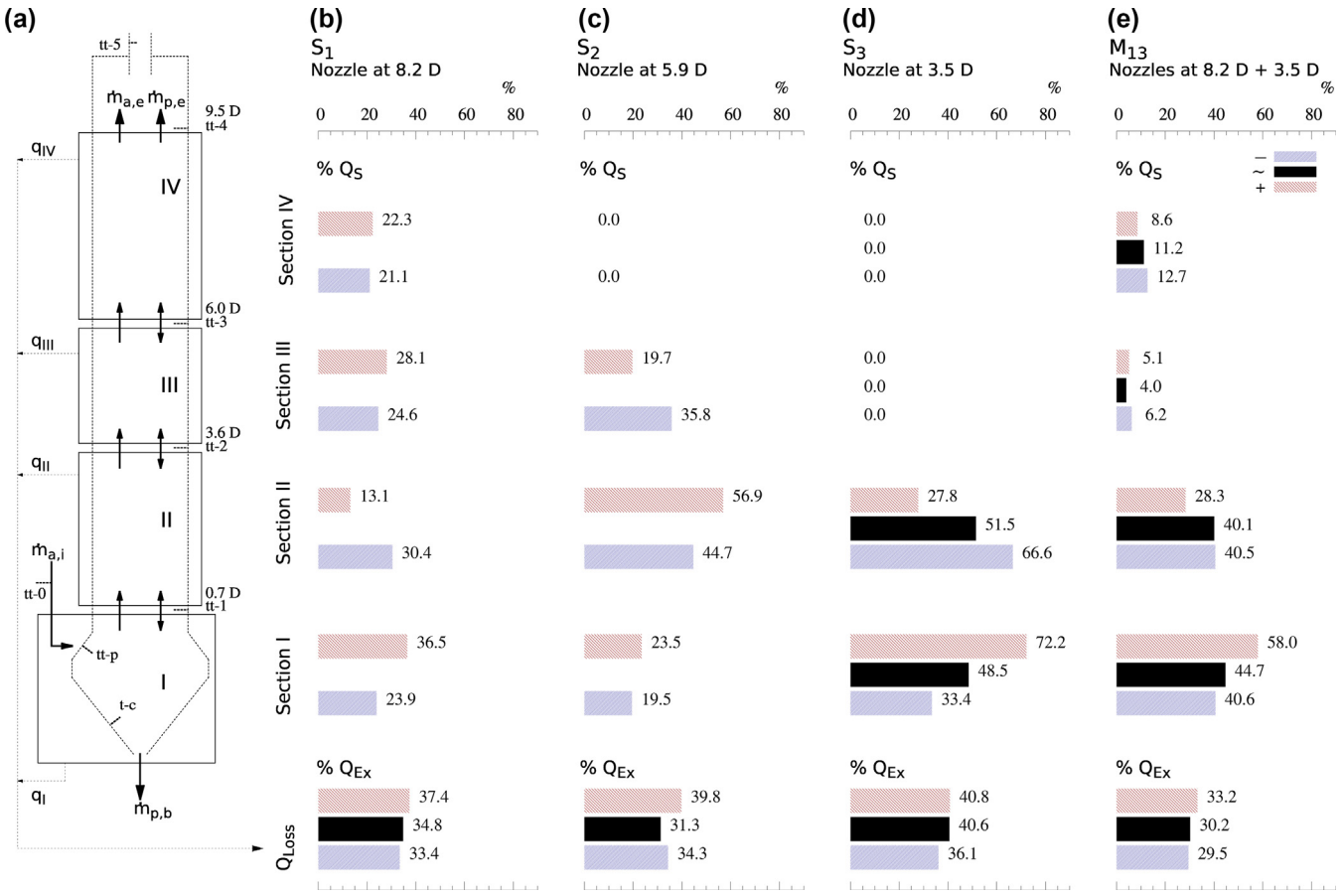

Fig. 6. (a) Definition of Section I, Section II (containing nozzle #3), Section III (containing nozzle #2) and Section IV (containing nozzle #1). Heat losses, Q_{Loss}, and distribution of the rate of heat transferred to the solids, Q_s (b) S_1, nozzle at 8.2 D (c) S_2, nozzle at 5.9 D (d) S_3, nozzle at 3.5 D, (e) M_{13}, nozzles at 8.2 D and 3.5 D.

is limited across the cylinder, is distributed according to the contact area of each section and the wall-air temperature difference assuming comparable heat transfer resistances. Assumptions on characteristic flow patterns and temperature profiles are made: 1 – air flows only upwards, 2 – above a nozzle droplets flow upwards, dry close to the spray and acquire the temperature of the air, 3 – below a nozzle droplets flow downwards and T_S increases linearly with distance to the exit value T_P. Since the contribution of heating $\Delta H_{P,sn}$ is low, $Q_{S,i}$ may be used as an indicator of the heat used for evaporation.

Fig. 6 shows how the energy input is utilised. The largest proportion of heat Q_S is exchanged in the cone, Section I. The proportion exchanged within the nozzle region varies from 21.1–22.3% in S_1 (Section IV) to 19.7–35.8% in S_2 (Section III) and 6.6–27.8% in S_3 at (Section II). It becomes more significant as the spray moves down because the droplets face higher air temperature and velocity, which increases ΔT and the powder residence time. A stronger vortex – drags the solids further up in the tower shifting the heat exchange into the cylindrical chamber. In turn, a weaker vortex + reduces the powder concentration and exchanges more of the heat at the bottom where the temperature is highest. In a two-level arrangement, M_{13}, a small fraction of the heat is exchanged between the nozzles or at the top, Fig. 6. It is an important observation for it shows that one cannot promote the heat transfer at the top spray in order to suppress particle growth simply by increasing the inlet air temperature. In fact, this is detrimental in M_{+13} because the high temperature shifts drying to the bottom end and as a result of the density increase the airflow cannot longer concentrate the powder at the top. In the largest units several nozzles are used in each level; rather than modifying the air flow, an alternative way to control heat transfer and agglomeration at the top can be adjusting the combined rate of all bottom nozzles changing their number but maintaining the droplet size.

4.5. Local drying conditions in the nozzle region(s)

To compare different regions and the tendency for the powder to deposit or agglomerate it is useful to compute specific heat transfer rates q, Table 3, particularly in the nozzle region(s). When velocity rises in S_{-2} and S_{-3}, the solids concentrate further up and convection is better; as a result q reaches the highest value within the nozzle region where the droplets contain the largest amount of water (Section III and Section II respectively). In turn, the weaker drag imposed by a hot vortex + makes the powder concentrate at lower positions and q reaches its highest value in the section below the spray, Section III in S_{+1}, Section II in S_{+2} and Section I for S_{+3}. When the nozzle is placed at the top in S_{-1}, the solids spend more time in the cylinder; more drying occurs before the air reaches the top and the temperature in the nozzle region, Section IV, drops (Fig. 5) reducing q, Table 3. In this case, the energy is homogeneously exchanged across the cylinder but a cold vortex fails to convey heat close the spray because it does not sustain the ΔT. Notice that during S_{-1} and S_{-2} the heat transfer rate q reaches fairly constant values at the bottom, Sections II and III. It may be consequence of the change in the droplet morphology; when the droplets initially shrink the drying rate is driven by heat transfer but after forming a porous crust it becomes dominated by internal

Table 3
Distributed energy balance. Thermal efficiency, η_t, and heat transfer efficiency, η_h. Bold indicates the spray region(s). Data for $M_{\sim 13}$ taken from Francia et al. (2016b).

Case	S_{-1}	S_{+1}	S_{-2}	S_{+2}	S_{-3}	$S_{\sim 3}$	S_{+3}	M_{-13}	$M_{\sim 13}$	M_{+13}
Overall Energy Balance										
Q_{Loss} (% Q_{Ex})	33.4 ± 1.1	37.4 ± 1.7	34.3 ± 0.9	39.8 ± 1.0	36.1 ± 0.7	40.6 ± 0.5	40.8 ± 1.0	29.5 ± 2.1	30.2 ± 1.8	33.2 ± 2.2
$\Delta H_{p,Sn}$ (% Q_{Ex})	−0.1 ± 1.6	1.3 ± 2.7	0.6 ± 1.4	1.2 ± 1.7	−0.9 ± 1.0	−1.5 ± 0.9	−0.4 ± 1.8	1.6 ± 3.0	−2.2 ± 2.7	1.5 ± 3.3
η_t [a]	0.72 ± 0.01	0.78 ± 0.01	0.73 ± 0.02	0.77 ± 0.03	0.66 ± 0.01	0.72 ± 0.02	0.74 ± 0.01	0.76 ± 0.02	0.79 ± 0.02	0.83 ± 0.02
η_h [b]	0.49 ± 0.01	0.50 ± 0.02	0.48 ± 0.01	0.47 ± 0.02	0.43 ± 0.01	0.43 ± 0.01	0.44 ± 0.01	0.55 ± 0.02	0.56 ± 0.02	0.57 ± 0.02
Specific drying rate, q kJ/s m kg^c_{DS}										
$II_{0.7\ D-3.6\ D}$	53.0 ± 0.5	22.3 ± 0.8	77.5 ± 0.4	99.5 ± 0.5	**108.3** ± 0.3	**77.0** ± 0.2	**43.8** ± 0.3	**69.5** ± 0.7	**70.6** ± 0.6	**46.9** ± 0.6
$III_{3.6\ D-6.0\ D}$	53.6 ± 0.3	59.7 ± 0.6	**77.6** ± 0.2	**43.1** ± 0.2	0.0	0.0	0.0	13.3 ± 0.4	8.8 ± 0.3	10.5 ± 0.3
$IV_{6.0\ D-9.5\ D}$	**30.5** ± 0.2	**31.6** ± 0.3	0.0	0.0	0.0	0.0	0.0	**18.1** ± 0.3	**16.5** ± 0.2	**11.9** ± 0.2

[a] Thermal efficiency $\eta_t = (T_{A,IN} - T_{A,EX})/(T_{A,IN} - T_{amb})$; [b] Heat transfer efficiency $\eta_h = Q_S/H_{A,IN}$; [c] Rate of heat transferred to the solids $q = Q_S/(\Delta z\ M_S\ (1 - X_{w,S}))$.

diffusion of water. In situ measurements of humidity and concentration would be necessary to establish the drying curve, but an early formation of a crust shortly after atomization could explain why q here responds to changes in residence time but not T_A.

Without sampling across the chamber or measuring in situ the powder water content or its mechanical properties, it is hard to establish unequivocally whether the differences in q within the nozzle region are sufficient to make the solids more or less sticky. However, combining the trends observed in Table 3 with the estimation of air velocity in Table 2 it is evident that the powder concentration in the nozzle region and thus the number of airborne contacts increases drastically in a strong cold vortex. As a result, one expects the agglomeration of dry particles concentrating near the wall with high velocity droplets coming from the spray to be heavily promoted in these areas.

4.6. Energy efficiency, a cold strong vortex vs a hot weak vortex

The heat transfer efficiency η_h (i.e. amount of energy transferred to the solids) obtained from a single nozzle remains constant as long as it is placed sufficiently high ($S_{\sim 1}$ and $S_{\sim 2}$) and only decreases when the residence time of the airborne powder reduces excessively from too low positions, $S_{\sim 3}$ (Francia et al., 2016a). As expected, increasing the temperature T_A and the concentration using two nozzle levels in $M_{\sim 13}$ renders a more efficient energy exchange (Francia et al., 2016b).

Table 3 summarizes the efficiency of different operation strategies. The use of a hot weak vortex + promotes the ΔT between the phases and increments the thermal efficiency η_t i.e. more heat is extracted from the air. However, it is not beneficial because it is owes to heating the dryer and increasing the losses Q_{Loss}. Remarkably, the heat transfer efficiency η_h i.e. the rate actually transferred to the solids, remains constant in Table 3, which means both strategies require the same energy input i.e. fuel, to dry the product to the same level. In a hot vortex + more of this energy is lost to the environment, Q_{Loss} while in a cold strong vortex − more energy leaves the system with the exhaust air enthalpy flow i.e. notice the exhaust air exits at a similar $T_{A,EX}$, Table 1, but in cases − it carries more mass. Both strategies are then equally efficient in terms of the overall use of energy but low temperatures are notably advantageous since they allow: (a) optimising capacity by creating fewer coarse granules, Table 1, which in effect also reduces the energy wasted in drying discarded powder (∼2% in Table 1) (b) potential improved designs; while the heat losses from the walls in the hot case + are irreversible, low temperatures allow for recovery of the exhaust air by recirculation into the burner (Golman and Julklang, 2014), which would cut down substantially the energy consumption, and finally (c) reduce the exposition of powder to high temperatures and thus avoid stability, safety and degradation issues opening the application to a wider range of formulas.

4.7. Wall deposition patterns

Most of the tower shows no deposits due to a low concentration i.e. top, or the dry state of the solids i.e. bottom. The highest rate corresponds to the projection of the spray(s). Table 4 summarizes the initial net deposition rate, $r_{d,o}$ and Fig. 7 shows selected areas. The transition between low to high velocities produces more deposits near the top spray in S_1 and M_{13}. A stronger drag shifts the trajectory of the spray upwards so that it covers more of the inspection area centred at 6.9 D i.e. see projection according to the spray angle in Fig. 2, 6.1–6.8 D. In the same way, the operation from nozzle #2 shows a decrease in S_{-2} because the projection may start to fall above the section considered. The same occurs in S_3 where particles are presumably drier when they reach the wall. It is important highlighting that $r_{d,o}$ represents the initial rate of deposition. At this stage, deposition is not balanced by resuspension and the deposits thicken at a constant rate. As this happens, the stresses sustained rise and the thickness stabilises but only after a long time (>60 min in $S_{\sim 2}$ Francia et al., 2015a). One must consider $r_{d,o}$ an indication of the rate of impacts to the wall, not the final thickness.

4.8. Evolution of particle size under different flow conditions

The changes in the elutriation rate, Table 1, show that the rate of powder flowing up increases drastically in a cold strong vortex. That implies that a fraction of the droplet population tends to

Table 4
Initial wall net deposition rate $r_{d,o}$ (g m^{-2} s^{-1}). Bold indicates the closest to the spray projection, depicted in Fig. 2. Data for the reference cases ∼ taken from Francia et al. (2016a, 2016b).

Level z/D	S_{-1}	$S_{\sim 1}$	S_{+1}	S_{-2}	$S_{\sim 2}$	S_{+2}	S_{-3}	$S_{\sim 3}$	S_{+3}	M_{-13}	$M_{\sim 13}$	M_{+13}
10.4	0.00	–	0.03	–	–	–	0.01	0	0.02	–	–	–
9.2	0	0	0	0.01	0.00	0	0	0	0	0.63	0.50	0.41
8.1	0.28	0	0.02	0.14	0.04	0.09	0.01	0	0.01	0.39	0.24	0.59
6.9	**0.75**	**0.91**	**1.48**	0	0.02	0.02	0.05	0.04	0.02	**1.04**	**1.37**	**1.47**
5.7	0	0	0	0	0	0	0	0	0.05	0	0	0.03
4.5	0	0	0	**1.00**	**1.81**	**1.26**	0.02	0	0	0	0	0
3.4	0	0	0	0	0	0	0	0.02	0	0	0	0
2.2	0	–	0	–	–	–	**0**	**0.01**	**0**	**–**	**0.06**	**–**

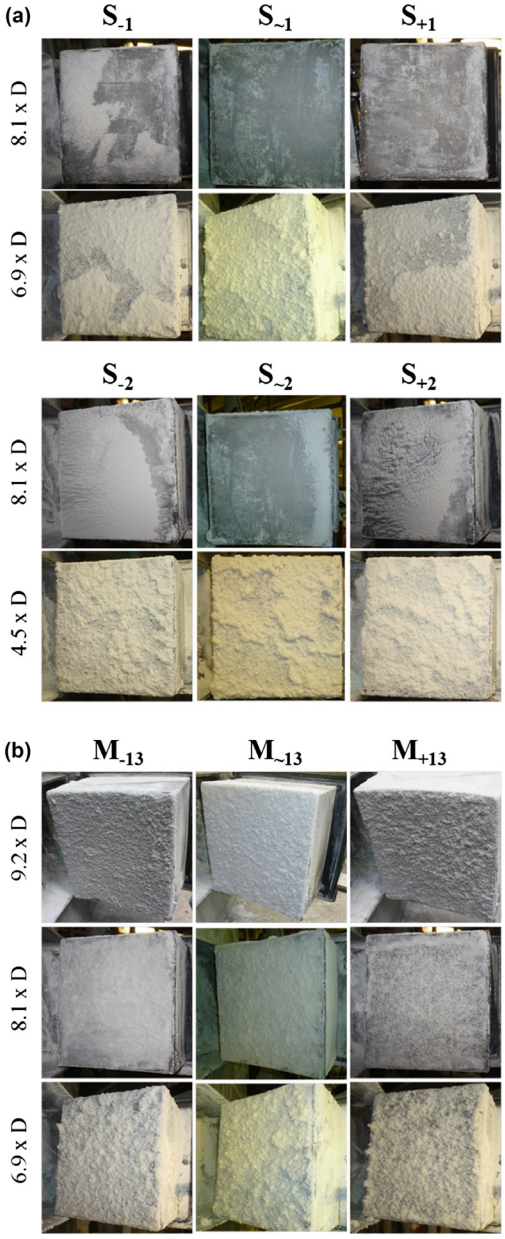

Fig. 7. Inspection of the wall at the top end and in the areas of spray projection. (a) S_1, S_2 and (b) M_{13}.

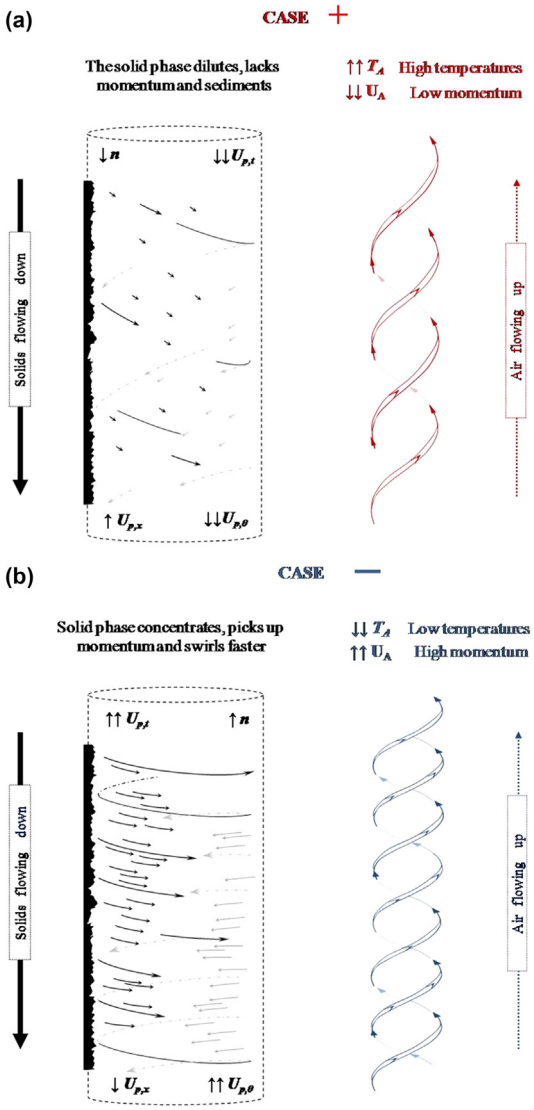

Fig. 8. Depiction of the change in concentration, dispersion and wall impacts during the transition from a weak hot vortex to a cold strong vortex (increasing velocity, reducing temperature) from cases + to −.

stagnate and therefore, concentration must be very sensitive to changes in air velocity. As it increases from the hot to the cold cases, the droplets concentrate further up and the areas where agglomerates form shift. It is important to recognise two differentiated effects in increasing air velocity, Fig. 8. In the axial direction, the drag opposes sedimentation and accumulates more powder at higher locations. In parallel, the azimuthal component of drag entrains the solids in a stronger swirl so that they reach overall a higher terminal velocity. The relative velocity at which air-borne particles fall and collide is due to different settling velocities (e.g. axial component of the terminal velocity) and it does not change substantially from the hot to the cold case, but when using a strong vortex the solids acquire a much higher tangential momentum and more of the powder is thrown to the walls with a higher energy. In turn, in a weak hot vortex less solids are held up, reducing the number of contacts and the kinetic energy carried by the powder.

Fig. 9 shows the overall increase in size comparing the droplet population to the product in a single nozzle case ($S_{\sim 3}$)

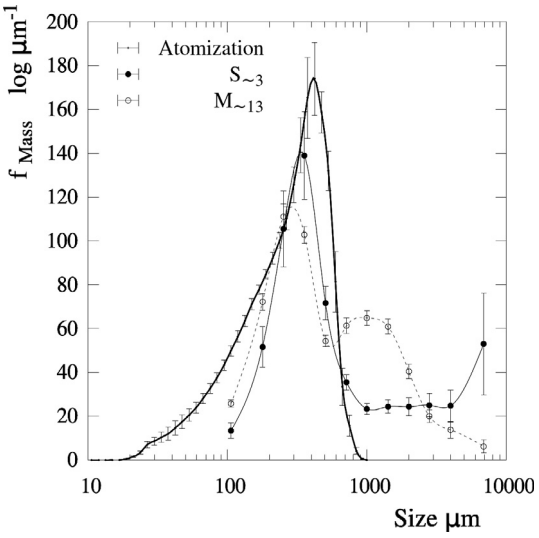

Fig. 9. Standard growth pattern. Comparison of the droplet size to $S_{\sim 3}$ (Francia et al., 2016a) and $M_{\sim 13}$ (Francia et al., 2016b).

characterised by mono-modal size distribution and generation of a coarse plateau (Francia et al., 2016a), and a two-level system ($M_{\sim 13}$) characterised by a bi-modal distribution where fine and coarse modes are associated to the bottom and top sprays respectively (Francia et al., 2016b). Our previous work correlated the growth pattern to the drying rate near the nozzle and quantified the interaction between sprays but it did not provide a way to relate size with air conditions. Fig. 10 shows how the product size can be manipulated with air temperature and velocity. A neat trend appears whereby increasing the flow velocity from a hot weak vortex + to a reference ∼ and a cold strong vortex − leads to a size reduction, particularly the granules >850 μm. The median product size $x_{p,50}$ and the higher percentiles $x_{p,90}$ drop significantly, Table 5. Fig. 10a shows how the transition from S_{+1} to S_{-1} reduces the number of coarse granules because agglomeration shifts to lower size range, turning the tail into a shoulder between 600 and 1180 μm in $S_{\sim 1}$ or into a secondary mode in S_{-1}. Fig. 10b and c shows similar tends: moving to higher velocities reduces the tail in S_{-2} or the plateau in S_{-3}.

One must comment on the possibility of the size reduction being consequence of better convective heat transfer and a higher drying rate near the nozzle, Table 3. Better heat transfer can make particles less prone to stick and it could have explained why the mean size reduces if there was a congruent evolution of the distribution. It is not the case. All experiments show a size reduction, while not all show an increased q. More importantly, better convection cannot explain why fewer granules >850 μm are formed. If air-borne solids were made less sticky they would generate fewer agglomerates and the distribution should shift to a lower size characteristic of the droplets. Potentially one expects to see the separation of particles that result from airborne contacts from those that come off the walls (perhaps the mode shifting to the left and a secondary mode appearing). Instead, one sees a reduction precisely in the population of granules that beyond any doubt come off the deposits. Figs. 10b and 1c provide sound evidence: the reduction in size responds to a change in the tail and involves the exact same set of granules that appear as a mixture of airborne droplets and deposited material in tracer experiments: x_p > 850 - μm in $S_{\sim 2}$ (Francia et al., 2015a).

The size reduces despite the solids accumulate further. This is particularly important near the wall and in the nozzle region (see Fig. 1a) where solids face high velocity droplets. When moving into a higher collision rate at higher momentum, creation of smaller particles is characteristic of breakage rather than agglomeration processes. Breakage shall occur close to the walls where particles concentrate and an impacts causes the highest stress e.g. at the wall the particles face the largest relative impact velocity. Such phenomenon is only consistent with the conclusions of visualization studies (Hassall, 2011) and tracer experiments that evidence resuspension of wallborne clusters (Francia et al., 2015a). To understand this dynamic it is helpful to think on an overall energy balance to the air. Drag transfers the air momentum to the solid phase, which is used to hold it up and increase momentum. Most of it reaches the wall and when it does, it transmits its kinetic energy to a loose structure of clusters shown in Fig. 1b and expanded in Fig. 11. Today there is no other alternative but simplifying these contacts with a restitution coefficient. This holds for static and thin deposits, but it can introduce gross errors when deposits are dynamic because it neglects the role of the microstructure i.e. change in particle size due to deposition/resuspension cycle or the effect in residence time of the time the particles spend rolling, saltating, locked or fixed at the wall.

It is important noticing that when one looks at *PIV* images, Fig. 11, all contacts present a similar mechanics. It is the time scale what defines whether a particle is "fixed" at the deposits and "wallborne" (greyed) or flowing and "airborne" (white). Most are

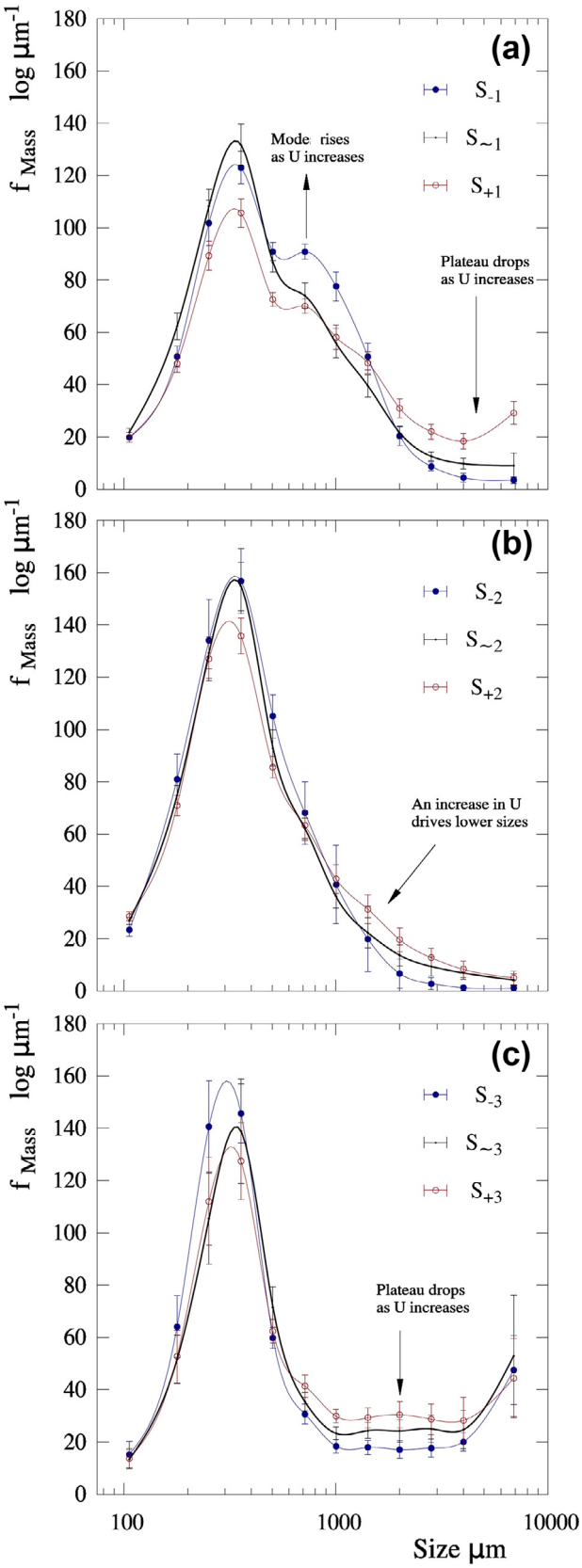

Fig. 10. Variation of the product size using a single nozzle from the reference cases (∼, black) (Francia et al., 2016a) to a hot weak vortex $\uparrow T_A \downarrow U_A^2$ (+, red) or a cold strong vortex $\downarrow T_A \uparrow U_A^2$ (−, blue) (Francia et al., 2015b), for (a) top spray #1, S_1, (b) middle spray #2, S_2 and (c) bottom spray #3, S_3. (For interpretation of the references to colour in this figure legend, the reader is referred to the web version of this article.)

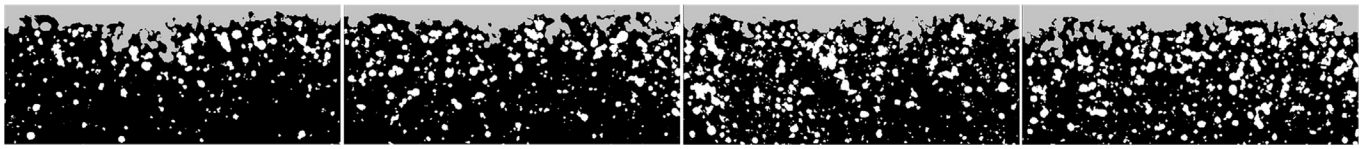

Fig. 11. Wall interactions under Particle Image Velocimetry, *PIV*, modified from Hassall (2011). Airborne powder appears as white; the deposited material and clusters in direct contact with it have been made grey. The wall deposits appear at the top, airborne particles are moving from left to right and towards the top due to centrifugal inertia.

either in contact to a particle at the wall or near to it and so they form a sort of loose structure. In fact, most clusters in Fig. 11 are highly non-spherical and tend to lock e.g. see top right Fig. 11. The way in which such a structure evolves must respond to the number and energy of the incoming impacts and the balance between the forces maintaining particle wallborne (greyed) i.e. capillary, viscous bridges, solid bridges, and the stress causing it to break up and start flowing i.e. gravity, impacts, aerodynamic. With this frame in mind, a size reduction is not surprising. In a hot weak vortex + the wall is subject to low stresses, low adhesion forces may be overcome and breakage shall produce fewer particles of a large size i.e. break up of fewer bonds. It may happen only when clusters grow sufficiently for gravity to make them detach. However, when the air velocity rises in a cold strong vortex – the structure sustains larger aerodynamic forces and bombardment of more particles at higher momentum, Table 2. This facilitates breakup of bonds and formation of smaller particles. In essence, increasing or decreasing the concentration and the kinetic energy of the solids modifies the wearing time scale and leads to either (a) a thin active layer resulting from frequent resuspension events of small fragments, or (b) a thick active layer originated from intermittent detachment of large pieces.

The same trend is observed in a multi-level system, Fig. 12, whereby the coarse size mode formed by the top spray shifts into a lower size at high air velocity. Fig. 13 includes the contribution to the powder in M_{13} originated by the top #1 and bottom nozzles #3, denoted M_1 and M_3, and compares them to the production from the same nozzles under a cold strong vortex, S_1 and S_3. At the bottom spray #3, Fig. 13a, the multi-level operation conditions M_3 inhibit particle growth because the air conveys more momentum and heat to the solids (U_{av} rises by 20–25% in Table 1, and q increases in Section II from 108.3 to 161.9 kJ/s m kg_{DS} Francia et al., 2016b); consequently the surface of particles becomes less prone to stick and the rate and energy of impacts promote breakage. At the top spray however, Fig. 13b, the size is not reduced in multi-level operation conditions, M_1 carries more momentum than S_{-1} (U_{av} rises 15% in Table 2) but it cannot maintain the drying rate among other things because the air humidity rises (i.e. q remains similar near the nozzle, Section IV at 30.5 and 29.6 kJ/s m kg_{DS}, but it decreases below, Section III, from 53.6 to 34.3 kJ/s m kg_{DS} Francia et al., 2016b). In this case, more powder was held up and more kinetic energy was transferred to the solids but the size rises presumably because drying was insufficient to prevent droplets to agglomerate both airborne and wallborne. These results showcase the importance of formulation and drying rate in the agglomeration kinetics. It cannot be exclusively controlled by the flow kinetic energy but it also responds to the equilibrium of deposits with local conditions e.g. temperature and humidity.

In summary, the combination of this work with *PIV* (Hassall, 2011) and tracer studies (Francia et al., 2015a) stresses the importance of wall interactions in particle formation during spray drying. The kinetic energy of the vortex controls the number and energy of the particles impacting deposit structures (Figs. 1b and 11) and the size of the clusters resuspended. The higher the disruptive stresses, the smaller fragments are generated but if particles move to the wall at low velocity they can lock, spend longer time in contact dry, sinter, and detach only when they grow sufficiently. In some senses, one can think on such dynamic as a reduction in cluster lifetime for increasing levels of turbulence. Wall agglomeration surely occurs in parallel with traditional sources of airborne particle growth (e.g. coalescence, multiple spray interactions). However, the ability of manipulating product size shown in Table 5 provides evidence of the importance of breakage and its potential to improve the performance of swirl dryers.

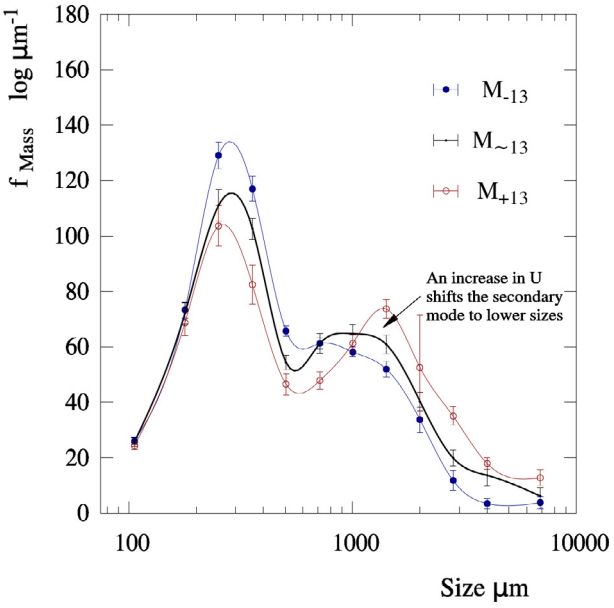

Fig. 12. Variation of the product size using two spraying levels from the reference case $M_{\sim 13}$ (black) (Francia et al., 2016b) to a hot weak vortex $\uparrow T_A \downarrow U_A^2$ in M_{+13} (+, red) or a cold strong vortex $\downarrow T_A \uparrow U_A^2$ in M_{-13} (−, blue). (For interpretation of the references to colour in this figure legend, the reader is referred to the web version of this article.)

Table 5
Reduction in exit product size. Droplets and reference cases ~ are taken from Francia et al. (2016a, 2016b). Intervals denote ±σ.

Case	x_{10}, µm	x_{25}, µm	x_{50}, µm	x_{75}, µm	x_{90}, µm
Droplets	85 ± 7	157 ± 10	292 ± 11	427 ± 9	530 ± 14
S_{+1}	185 ± 7	290 ± 12	546 ± 47	1352 ± 153	4463 ± 560
$S_{\sim 1}$	173 ± 4	261 ± 7	413 ± 15	824 ± 64	1724 ± 286
S_{-1}	183 ± 7	278 ± 8	458 ± 28	862 ± 50	1438 ± 123
S_{+2}	158 ± 3	239 ± 5	371 ± 14	684 ± 66	1443 ± 214
$S_{\sim 2}$	161 ± 3	238 ± 5	360 ± 10	597 ± 53	1168 ± 232
S_{-2}	166 ± 6	239 ± 14	359 ± 33	565 ± 93	901 ± 180
S_{+3}	198 ± 16	283 ± 26	508 ± 157	2145 ± 1128	x_{86} = 4760
$S_{\sim 3}$	195 ± 12	282 ± 20	456 ± 98	2224 ± 1575	x_{83} = 4760
S_{-3}	187 ± 14	258 ± 16	388 ± 39	1670 ± 1062	x_{84} = 4760
M_{+13}	166 ± 3	254 ± 8	541 ± 63	1464 ± 146	2761 ± 216
$M_{\sim 13}$	163 ± 3	246 ± 6	423 ± 22	1093 ± 61	2023 ± 186
M_{-13}	162 ± 3	240 ± 4	383 ± 13	858 ± 76	1606 ± 160

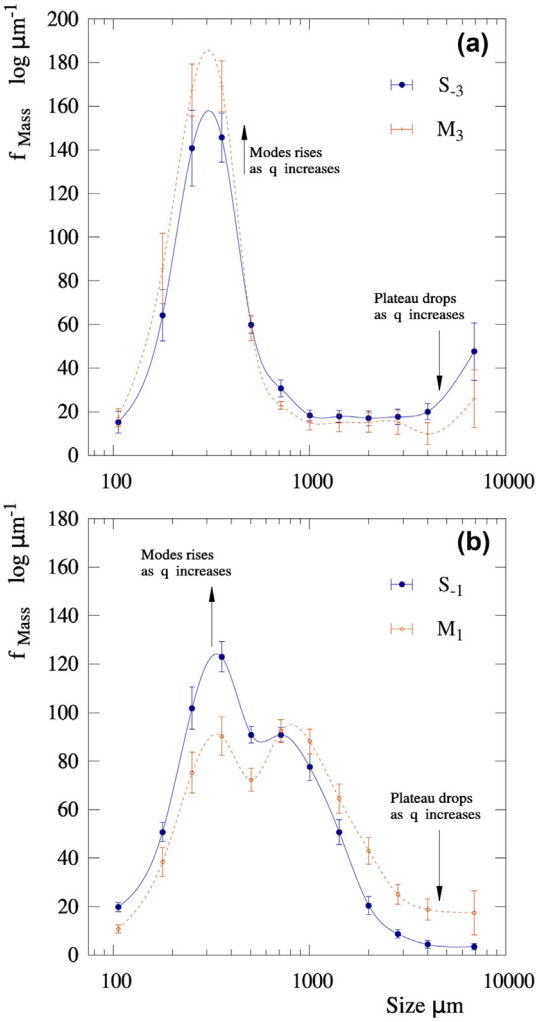

Fig. 13. Comparison of the product size resulting from nozzles #1 and #3 in multi-level operation conditions, M_1 and M_3 (Francia et al., 2016b) to under a cold strong vortex $\downarrow T_A \uparrow U_A^2$ (−, blue), S_{-1} and S_{-3}. (a) Bottom nozzle #3, M_3 and S_3, (b) top nozzle #1, M_1 and S_1. (For interpretation of the references to colour in this figure legend, the reader is referred to the web version of this article.)

4.9. Drying history. Sensitivity of water content to particle size

The product exit water content X_w is a strong function of particle size. In the reference cases, the higher water content in fine and coarse fractions was related to the fast sedimentation of coarse granules and their breakage into particles <212 µm (Francia et al., 2016a, 2016b). It was also underscored that the bulk water content was rather insensitive to a change in flow pattern or temperature history perhaps due to the time the solids dry at the wall. Fig. 14 confirms these observations. Cold and hot experiments are adjusted to cause the same evaporation, and with the exception of S_3 all present a similar exit bulk water content. However, given the large difference in the temperature (Fig. 4) and the axial drag (Table 2) faced by the powder, it is interesting to find no differences in on how water distributes across different sizes, Fig. 14. All cases show the same profile and large particles exhibit a similar content. It is particularly remarkable for the hot cases + where granules >1800 µm are expected to spend barely few seconds flowing. The wall dynamic can explain this lack of sensitivity. The relation expected between size and water content owes to the time particles are flowing. Considering that most of them come off the wall and that they dry at the deposits for much longer i.e. 2–30 min (Francia et al., 2015a), than what they remain airborne

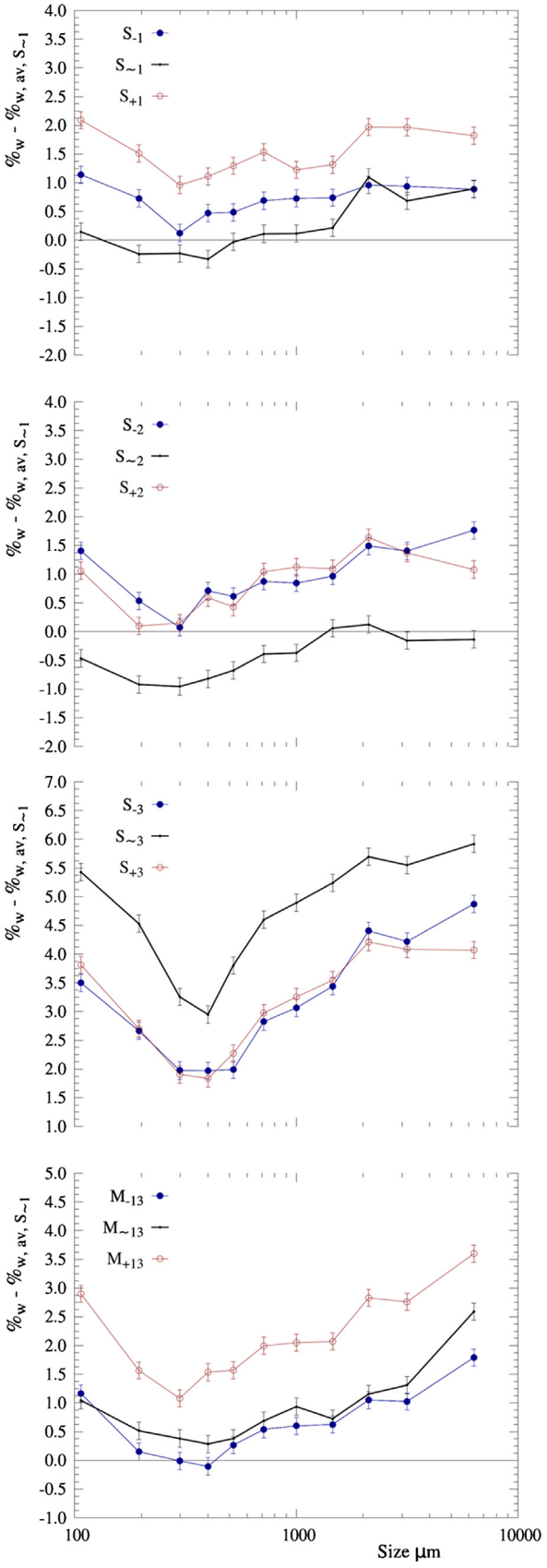

Fig. 14. Product water content X_W. (a) S_1, (b) S_2, (c) S_3 and (d) M_{13}. Comparison of reference productions (∼, Francia et al., 2016a, 2016b black) to a hot weak vortex $\uparrow T_A \downarrow U_A^2$ (+, red) and a cold strong vortex $\downarrow T_A \uparrow U_A^2$ (−, blue). (For interpretation of the references to colour in this figure legend, the reader is referred to the web version of this article.)

from removal to exit <5–45 s (Ali et al., in press), one must associate the final water content to the one when resuspension was triggered, in other words, the moisture at which a wall cluster can be worn off. Wearing cannot occur at any condition, when drag, gravity or a particle impact imposes a stress in the deposit structure (dry erosion mechanisms, Francia et al., 2015a), resuspension occurs only if the clusters have turned to some extent elastic, otherwise they simply deform, consolidate or smear. Similarly, for a cluster to be picked up by a wet droplet at high momentum (wet erosion mechanisms, Francia et al., 2015a) the structure must have become to some extent non-deformable to transmit the stress. The interplay between resuspension rate and deposit water content can explain why particles must remain for some time at the wall before being removed and why X_w content is relatively insensitive to the airborne temperature history.

5. Conclusions

This work has investigated the role that wall clustering in the operation of swirl dryers and the benefits of different control strategies based in manipulation of air temperature and velocity. High temperatures result in better heat transfer near the nozzles only when they are located sufficiently high in a dryer. When multiple levels are used or when nozzles are brought to the bottom, the role of the air velocity in concentrating the powder has a dominant effect and a strong vortex is the btter way to promote drying near the sprays. Most importantly, increasing the momentum of the flow inhibits the creation of coarse aggregates i.e. >850 μm. This trend appears to be independent of production rate, nozzle location or operation of single or multiple levels. It is very relevant because it indicates that growth is to some extent dominated by the rate of breakage of wall clusters and the stresses sustained by the deposit microstructure.

A correlation between growth and the energy of wall impacts along with the works of Hassall, 2011 and Francia et al., 2015a demonstrate that fouling is intimately related to agglomeration in detergent spray drying. It appears that swirl towers operate, quite remarkably, by bringing the powder in contact to and near the wall and then breaking up the clusters generated with the energy obtained from the swirl. Indeed, this represents an important leap in the traditional paradigm (Huntington, 2004), but one must recognise that past studies lack sufficient knowledge of fouling, focused in past formulations and large towers where many nozzles are used, thus confounding other sources of growth with the wall. Optimisation must start focusing in describing the dynamic of fouling in terms of a balance between operation conditions and deposit microstructure: how cohesive forces evolve when clusters dry and sinter at the wall and when the stresses due to drag, gravity and incoming impacts are sufficient to break them. The size reduction achieved here changing the air inlet conditions shows significant potential to improve performance. New designs concepts based in usage of low temperature and exhaust recirculation promise a greater ability to control the product size, avoid operational issues and recover energy losses.

The series of works described here represents the first attempt to quantify the dynamic nature of deposits in any dryer. It has been proven that the traditional approach that envisaged deposits as static matter needs to be reconsidered in swirl counter-current towers and detergent formulations. One can only speculate how important dynamic fouling may be when drying other formulas and/or using other chambers e.g. nil-swirl, co-current, that tend to generate deposits. These are also traditionally considered static matter but one must notice that reaching an equilibrium weight is not proof that deposits are static or that they do not influence the process. On the contrary this work shows that a cycle of deposition and resuspension may still be at the core of the process. Unless the wall residence time and the resuspension rate are tracked experimentally one simply does not know how relevant the walls may be. Similar quantitative tracer analysis to the one reported in Francia et al. (2015a) could help clarifying the nature of fouling in other drying chambers, process conditions or formulations.

Acknowledgments

VF was supported by an Engineering Doctorate Studentship sponsored by the Engineering and Physical Sciences Research Council (EPSRC) and Procter & Gamble in the Industrial Doctoral Centre in Formulation Engineering, School of Chemical Engineering, University of Birmingham. The authors also want to particularly thank Dr. Guy Hassall for providing access to *PIV* experimentation and his valuable advice in the early stage of this programme.

References

Abd-Elhady, M.S., Clevers, S.H., Adriaans, T.N.G., Rindt, C.C.M., Wijers, J.G., Steenhoven, A.A., 2007. Influence of sintering on the growth rate of particulate fouling layers. Int. J. Heat Mass Transf. 50, 196–207.

Adamczyk, Z., Weronski, P., Barbasz, J., 2008. Formation of multilayered structures in the layer by layer deposition of colloid particles. J. Colloid Interface Sci. 317, 1–10.

Adhikari, B., Howes, T., Bhandar, B.R., Troung, V., 2003. In situ characterization of stickiness of sugar-rich foods using a linear actuator driven stickiness testing device. J. Food Eng. 58, 11–22.

Adhikari, B., Howes, T., Lecomte, D., Bhandari, B., 2005. A glass transition temperature approach for the prediction of the surface stickiness of a drying droplet during spray drying. Powder Technol. 149 (2), 168–179.

Ali, M., Mahmud, T., Heggs, P.J., Ghadiri, M., Bayly, A., Ahmadian, H., Martin de Juan, L., 2016. CFD modelling of a pilot-scale counter-current spray drying tower for the manufacture of detergent powder (in press). http://dx.doi.org/10.1080/07373937.2016.1163576.

Ali, M., Mahmud, T., Heggs, P.J., Ghadiri, M., Bayly, A., Crosby, M., Ahmadian, H., Martin de Juan, L., Zayeed, A., 2017. Residence time distribution of glass ballotini in isothermal swirling flows in a counter-current spray drying tower. Powder Technol. 305, 809–815.

Alipour, M., Kurian, V., Dhir, S., Gupta, R., 2016. Analysis of syngas cooler fouling from asphaltene gasification. Fuel Process. Technol. 152, 7–14.

Alves, A., Paiva, J., Romualdo Salcedo, R., 2015. Cyclone optimization including particle clustering. Powder Technol. 272, 14–22.

Bansal, B., Chen, X.D., 2006. A critical review of milk fouling in heat exchangers. Compr. Rev. Food Sci. Food Saf. 5 (2), 27–33.

Barth, T., Reiche, M., Bankowski, M., Oppermann, M., Hampel, U., 2013. Experimental investigation of multilayer particle deposition and resuspension between periodic steps in turbulent flows. J. Aerosol Sci. 64, 111–124.

Batys, P., Nosek, M., Weronski, P., 2015. Structure analysis of layer-by-layer multilayer films of colloidal particles. Appl. Surf. Sci. 332, 318–327.

Boonyai, P., Bhandaria, B., Howes, T., 2004. Stickiness measurement techniques for food powders: a review. Powder Technol. 145, 34–46.

Bourrier, F., Nicota, F., Darve, F., 2010. Evolution of the micromechanical properties of impacted granular materials. C.R. Mec. 338, 639–647.

Chu, H.P., Li, X.Y., 2005. Membrane fouling in a membrane bioreactor (MBR): sludge cake formation and fouling characteristics. Biotechnol. Bioeng. 90 (3), 323–331.

Crüger, B., Salikov, V., Heinrich, S., Antonyuk, S., Sutkar, V.S., Deen, N.G., Kuipers, J.A. M., 2016. Coefficient of restitution for particles impacting on wet surfaces: an improved experimental approach. Particuology 25, 1–9.

Davis, R.P., Haines, M.S., Sagel, J.A., 1971. Multilevel Spray-Drying Apparatus. US Patent 3, December 28 1971, 629, 955. The Procter & Gamble Company. Cincinnati, Ohio.

Diaz-Bejarano, E., Coletti, F., Macchietto, S., 2016. A new dynamic model of crude oil fouling deposits and its application to the simulation of fouling-cleaning cycles. AIChE J. 62 (1), 90–107.

Fieg, G., Wozny, G., Buick, K., Jeromin, L., 1994. Estimation of the drying rate and moisture profiles in an industrial spray dryer by means of experimental investigations and a simulation study. Chem. Eng. Technol. 17, 235–241.

Focke, C., Kuschel, M., Sommerfeld, M., Bothe, D., 2013. Collision between high and low viscosity droplets: direct numerical simulations and experiments. Int. J. Multiph. Flow 56, 81–92.

Francia, V., Martin, L., Bayly, A.E., Simmons, M.J.H., 2015a. The role of wall deposition and re-entrainment in swirl spray dryers. AIChE J. 61 (6), 1804–1821.

Francia, V., Martin, L., Bayly, A.E., Simmons, M.J.H., 2015b. Particle aggregation in large counter-current spray drying towers: nozzle configuration, vortex momentum and temperature 7th World Congress in Particle Technology WCPT, Beijing, P.R. China, 2014 Procedia Eng. 102, 668–675.

Francia, V., Martin, L., Bayly, A.E., Simmons, M.J.H., 2015c. An experimental investigation of the swirling flow in a tall-form counter-current spray dryer. Exp. Therm. Fluid Sci. 65, 52–64.
Francia, V., Martin, L., Bayly, A.E., Simmons, M.J.H., 2015d. Influence of wall friction on flow regimes and scale up of swirl spray dryers. Chem. Eng. Sci. 134, 399–413.
Francia, V., Martin, L., Bayly, A.E., Simmons, M.J.H., 2016a. Agglomeration in counter-current spray drying towers, Part A: particle interactions and the effect of the nozzle height. Powder Technol. 301, 1330–1343.
Francia, V., Martin, L., Bayly, A.E., Simmons, M.J.H., 2016b. Agglomeration in counter-current spray drying towers, Part B: interaction between multiple spraying levels. Powder Technol. 301, 1344–1358.
Fries, L., Antonyuk, S., Heinrich, S., Dopfer, D., Palzer, S., 2013. Collision dynamics in fluidised bed granulators: a DEM-CFD study. Chem. Eng. Sci. 86 (4), 108–123.
Gianfrancesco, A., Turchiuli, C., Dumoulin, E., Palzer, S., 2009. Prediction of powder stickiness along spray drying process in relation to agglomeration. Part. Sci. Technol. 27 (5), 415–427.
Golman, B., Julklang, W., 2014. Analysis of heat recovery from a spray dryer by recirculation of exhaust air. Energy Convers. Manage. 88, 641–649.
Handscomb, C.S., Kraft, M., 2010. Simulating the structural evolution of droplets following shell formation. Chem. Eng. Sci. 65, 713–725.
Hanus, M.J., Langrish, T.A.G., 2007a. Re-entrainment of wall deposits from a laboratory-scale spray dryer. Asia-Pac. J. Chem. Eng. 2, 90–107.
Hanus, M.J., Langrish, T.A.G., 2007b. Resuspension of wall deposits in spray dryers. J. Zhejiang Univ. Sci. A 8 (11), 1762–1774.
Harris, A.R., Davidson, C.I., 2009. A Monte Carlo model for soil particle resuspension including saltation and turbulent fluctuations. Aerosol Sci. Technol. 43, 161–173.
Harvie, D.J.E., Langrish, T.A.G., Fletcher, D.F., 2001. Numerical simulations of the gas flow patterns within a tall form spray dryer. Trans. IChemE 79, 235–248.
Harvie, D.J.E., Langrish, T.A.G., Fletcher, D.F., 2002. A computational fluid dynamics study of a tall-form spray dryer. Trans. IChemE 80 (Part C), 163–175.
Hassall, G., 2011. Wall Build Up in Spray Driers EngD thesis. Chemical Engineering. University of Birmingham, Birmingham. United Kingdom.
Hastie, D.B., 2013. Experimental measurement of the coefficient of restitution of irregular shaped particles impacting on horizontal surfaces. Chem. Eng. Sci. 101, 828–836.
Henry, C., Minier, J.P., 2014. Progress in particle resuspension from rough surfaces by turbulent flows. Prog. Energy Combust. Sci. 45, 1–53.
Henry, C., Minier, J.P., Lefevre, G., 2012. Towards a description of particulate fouling: from single particle deposition to clogging. Adv. Colloid Interface Sci. 185–186, 34–76.
Huntington, D.H., 2004. The influence of the spray drying process on product properties. Drying Technol. 22 (6), 1261–1287.
Iimura, K., Watanabe, S., Michitaka Suzuki, M., Hirota, H., Higashitani, K., 2009. Simulation of entrainment of agglomerates from plate surfaces by shear flows. Chem. Eng. Sci. 64, 1455–1461.
Jaskulski, M., Wawrzyniak, P., Zbiciński, I., 2015. CFD model of particle agglomeration in spray drying. Drying Technol. 33 (15–16), 1971–1980.
Jin, Y., Chen, X.D., 2010. A fundamental model of particle deposition incorporated in CFD simulations of an industrial milk spray dryer. Drying Technol. 28 (8), 960–971.
Keshani, S., Montazeri, M.H., Daud, W.R.W., Nourouzi, M.M., 2015. CFD modeling of air flow on wall deposition in different spray dryer geometries. Drying Technol. 33 (7), 784–795.
Keshani, S., Daud, W.R.W., Nourouzi, M.M., Namvar, F., Mostafa, G., 2015. Spray drying: an overview on wall deposition, process and modelling. J. Food Eng. 146, 152–162.
Kota, K., Langrish, T.A.G., 2006. Fluxes and patterns of wall deposits for skim milk in a pilot-scale spray dryer. Drying Technol. 24 (8), 993–1001.
Kota, K., Langrish, T., 2007. Prediction of deposition patterns in a pilot-scale spray dryer using computational fluid dynamics (CFD) simulations. Chem. Prod. Process Model 2, 3.
Kuriakose, R., Anandharamakrishnan, C., 2010. Computational fluid dynamics (CFD) applications in spray drying of food products. Trends Food Sci. Technol. 21, 383–398.
Kuschel, M., Sommerfeld, M., 2013. Investigation of droplet collisions for solutions with different solids content. Exp. Fluids 54, 1440.
Langrish, T.A., 2009. Multi-scale mathematical modelling of spray dryers. J. Food Eng. 93, 218–228.
Lecrivain, G., Barry, L., Hampel, U., 2014. Three-dimensional simulation of multilayer particle deposition in an obstructed channel flow. Powder Technol. 258, 134–143.
Li, S., Marshall, J.S., Liu, G., Yao, Q., 2011. Adhesive particulate flow: the discrete-element method and its application in energy and environmental engineering. Prog. Energy Combust. Sci. 37, 633–668.
Lustfeld, M., Qu, T., Lippmann, W., Hurtado, A., Göhler, D., 2014. Experimental study of graphite particle deposition upstream of a forward-facing step. Nucl. Eng. Des. 271, 552–559.
Malafronte, L., Ahrnéa, L., Innings, F., Jongsma, A., Rasmuson, A., 2015. Prediction of regions of coalescence and agglomeration along a spray dryer -Application to skim milk powder. Chem. Eng. Res. Des. 104, 703–712.
Marshall, J.S., Renjitham, S., 2014. Simulation of particulate fouling at a microchannel entrance region. Microfluid. Nanofluid. 18 (2), 253–265.
Melián-Martel, N., Sadhwani, J.J., Malamis, S., Ochsenkühn-Petropoulou, M., 2012. Structural and chemical characterization of long-term reverse osmosis membrane fouling in a full scale desalination plant. Desalination 305, 44–53.
Mezhericher, M., Levy, A., Borde, I., 2008. Heat and mass transfer of single droplet/wet particle drying. Chem. Eng. Sci. 63 (1), 12–23.
Mezhericher, M., Levy, A., Borde, I., 2012. Probabilistic hard-sphere model of binary particle–particle interactions in multiphase flow of spray dryers. Int. J. Multiph. Flow 43, 22–38.
Nakazato, T., 2015. Multilayer adhering model for holdup and separation behavior of fine particles in a powder-particle fluidized bed. Powder Technol. 274, 289–295.
Nijdam, J.J., Guo, B., Fletcher, D.F., Langrish, T.A., 2006. Lagrangian and Eulerian models for simulating turbulent dispersion and coalescence of droplets within a spray. Appl. Math. Model. 30, 1196–1211.
Paiva, J., Romualdo Salcedo, R., Araujo, P., 2010. Impact of particle agglomeration in cyclones. Chem. Eng. J. 162, 861–876.
Palzer, S., 2009. Influence of material properties on the agglomeration of water-soluble amorphous particles. Powder Technol. 189, 318–326.
Palzer, S., 2011. Agglomeration of pharmaceutical, detergent, chemical and food powders. Similarities and differences of materials and processes. Powder Technol. 206, 2–17.
Palzer, S., Dubois, C., Gianfrancesco, A., 2012. Generation of product structures during drying of food products. Drying Technol.: Int. J. 30 (1), 97–105.
Pawar, S.K., Henrikson, F., Finotello, G., Padding, J.T., Deen, N.G., Jongsm, A., Innings, F., Kuipers, J.A.M.H., 2016. An experimental study of droplet-particle collisions. Powder Technol. 300, 157–163.
Sadripour, M., Rahimi, A., Hatamipour, M.S., 2012. Experimental study and CFD modeling of wall deposition in a spray dryer. Drying Technol. 30 (6), 574–582.
Soldati, A., Marchioli, C., 2009. Physics and modelling of turbulent particle deposition and entrainment: review of a systematic study. Int. J. Multiph. Flow 35, 827–839.
Sommerfeld, M., 2001. Validation of a stochastic Lagrangian modeling approach for interparticle collisions in homogeneous isotropic turbulence. Int. J. Multiph. Flow 27, 1829–1858.
Song, J., Xu, D., Wei, Y., 2016. Carbonaceous deposition onto the outer surface of vortex finder of commercial RFCC cyclones and role of gas flow to the buildup of the deposits. Chem. Eng. J. 303, 109–122.
Sutkar, V.S., Deen, N.G., Padding, J.T., Kuipers, J.A.M., Salikov, V., Crüger, B., Antonyuk, S., Heinrich, S., 2015. A novel approach to determine wet restitution coefficients through a unified correlation and energy analysis. AIChE J. 61 (3), 769–779.
Tan, H.S., Salman, A.D., Hounslow, M.J., 2006. Kinetics of fluidized bed melt granulation—II: modelling the net rate of growth. Chem. Eng. Sci. 61, 3930–3941.
Tanaka, K., Nishida, M., Kunimochi, T., Takagi, T., 2002. Discrete element simulation and experiment for dynamic response of two-dimensional granular matter to the impact of a spherical projectile. Powder Technol. 124, 160–173.
Verdurmen, R.E.M., Menn, P., Ritzert, J., Blei, S., Nhumaio, G.C.S., Sørensen, T.S., Gunsing, M., Straatsma, J., Verschueren, M., Sibeijn, M., Schulte, G., Fritsching, U., Bauckhage, K., Tropea, C., Sommerfeld, M., Watkins, A.P., Yule, A.J., Schønfeldt, H., 2004. Simulation of agglomeration in spray drying installations: the EDECAD project. Drying Technol. 22 (6), 1403–1461.
Wang, S., Langrish, T.A., 2009. A review of process simulations and the use of additives in spray drying. Food Res. Int. 42 (1), 13–25.
Wawrzyniak, P., Podyma, M., Zbicinski, I., Bartczak, Z., Rabaeva, J., 2012. Modeling of air flow in an industrial counter-current spray drying tower. Drying Technol. 30, 217–224.
Werner, S.R.L., Jones, J.R., Paterson, A.H.J., 2007. Stickiness of maltodextrins using probe tack test during in situ drying. J. Food Eng. 80, 859–868.
Woo, M.W., Daud, W.R.W., Mujumdar, A.S., Tasirin, S.M., Talib, M.Z.M., 2010. Role of rheological characteristics in amorphous food particle-wall collisions in spray drying. Powder Technol. 198, 252–257.
Yeap, B.L., Wilson, D.I., Polley, G.T., Pugh, S.J., 2004. Mitigation of crude oil refinery heat exchanger fouling through retrofits based on thermo-hydraulic fouling models. Chem. Eng. Res. Des. 82 (1), 53–71.
Zbicinski, I., Piatkowski, M., 2009. Continuous and discrete phase behavior in counter current spray drying. Drying Technol. 27 (12), 1353–1362.
Zbicinski, I., Strumillo, C., Delag, A., 2002. Drying kinetics and particle residence time in spray drying. Drying Technol. 20 (9), 1751–1768.
Zbicinski, I., Delag, A., Strumillo, C., Adamiec, J., 2002. Advanced experimental analysis of drying kinetics in spray drying. Chem. Eng. J. 86, 207–216.
Zbogar, A., Frandsen, F., Jensen, P.A., Glarborg, P., 2009. Shedding of ash deposits. Prog. Energy Combust. Sci. 35, 31–56.
Zhang, F., Reeks, M.W., Kissane, M.P., Perkins, R.J., 2013. Resuspension of small particles from multilayer deposits in turbulent boundary layers. J. Aerosol Sci. 66, 31–61.
Ziskind, G., 2006. Particle resuspension from surfaces: revisited and re-evaluated. Rev. Chem. Eng. 22, 1–123.